Material Characterization of Guadua Bamboo and the Environmental Feasibility of Structural Bamboo Products

by

Arfa N. Aijazi

Submitted to the
Department of Materials Science and Engineering
in Partial Fulfillment of the Requirements for the Degree of

Bachelor of Science

at the

Massachusetts Institute of Technology

June 2013

Signature of Author……
Department of Materials Science and Engineering
May 9, 2013

Certified by ……...
Lorna J. Gibson
Matoula S. Salapatas Professor of Materials Science and Engineering
Thesis Supervisor

Accepted by ……...
Jeffrey C. Grossman
Carl Richard Soderberg Associate Professor of Power Engineering
Chairman, Undergraduate Committee

Material Characterization of Guadua Bamboo and the Environmental Feasibility of Structural Bamboo Products

by

Arfa N. Aijazi

Submitted to the Department of Materials Science and Engineering
on May 9, 2013 in partial fulfillment of the requirements for the
degree of Bachelor of Science in Materials Science and Engineering

Abstract

Bamboo has long been used in vernacular construction because of its high strength, rapid growth rate, and global abundance. Bamboo is increasingly being used in contemporary architecture as a sustainable alternative to wood and other building materials. Forming bamboo into a structural composite can improve mechanical performance, durability, and joining, which can open up new structural applications and design possibilities as well as remove the stigma that bamboo is the "poor man's timber". This study aims to characterize the radial and longitudinal variation in the microstructure and mechanical properties of Guadua bamboo (*Guadua angustifolia kunth*) in order to inform efficient material use in a composite. The study found a linear relationship between the MOE, MOR, and compression strength with density. Through analysis of micrographs, the density was correlated to the area fraction of sclerenchyma fiber sheaths. Results from nanoindentation confirmed that the fiber properties did not vary with position. Further the environmental impact in the form of exhaustion of energy found that processed bamboo had a mechanical advantage over raw bamboo culm and lower energy input in manufacturing but superior performance in comparison to wood composites.

Thesis Supervisor: Lorna J. Gibson

Title: Matoula S. Salapatas Professor of Materials Science and Engineering

Acknowledgements

I wish to acknowledge the following individuals for their contributions that made this thesis project possible:

- Professor Lorna J. Gibson for introducing this project to me nearly two years ago and for her guidance and mentorship throughout that time
- Patrick Dixon for training me on the Instron and for his assistance and advice on sample preparation and experimentation
- Elsa Olivetti for her support and feedback on the environmental feasibility of SBP
- Alan Schwartzmann for training me on the nanoindentor and going above and beyond to ensure I had sufficient data for analysis
- Michael Ramage for the opportunity to continue working on the bamboo project at the University of Cambridge during my study abroad in Spring 2012
- Don Galler and Zack Cordero for training me on the scanning electron microscope
- Mike Tarkanian, Ike Felter, and Christopher Pema from the Department of Materials Science and Engineering for their help in using equipment in the Laboratory for Engineering Materials (LEM) and the waterjet
- Ken Stone, Hayami Arakawa, and Brian Chan at the MIT Hobby Shop for their assistance in machining bamboo for sample preparation

Table of Contents

List of Figures

List of Tables

Introduction

Bamboo is a subfamily of the true grass family Poacae and is among the fastest growing plants in the world. Bamboos have a broad natural distribution extending from latitudes of 46 °N to 47 °S and altitudes from sea level up to 4700 m, Figure 1. There are 10 genera of bamboos containing nearly 1500 species (Gratani, et al. 2008). Bamboos can be classified as herbaceous or woody. As the name suggests, like wood, woody bamboos have a high strength to weight ratio and are frequently used in construction, and are the primary interest of this study.

Figure 1: Global distribution of herbaceous bamboo, solid green, and woody bamboo, tan hashes, (Gardner and Vogel 2006)

Bamboo as a Construction Material and Structural Bamboo Composites

Indigenous groups in Central and South America, Asia, and Africa have historically used woody bamboos culms in their traditional construction, Figure 2. The emergence and increased availability of new construction materials around the world such as concrete and steel has caused a cultural shift in these societies. These new materials are perceived as being more solid and strong and have become a symbol of higher social and economic status. Those who could afford it abandoned indigenous materials and architectural practices in favor of the new materials. Today, only the poor in rural areas where bamboo grows continue to utilize bamboo construction. Bamboo is inexpensive because it grows rapidly and is locally available. As a consequence, bamboo

is seen as the "poor man's timber" and is not seen as a desirable construction material; instead its use is seen as necessitated by poverty. As such, many of these cultures have also developed myths to discourage the use of bamboo. For instance, in Indonesia, there is a belief that bamboo encourages snakes and in Thailand, a belief that bamboo brings bad spirits (Garcia-Saenz 2012).

Figure 2: Straw-covered bamboo huts of the Akha Meuo tribe in the traditional mountain village of Ban Chakhampa, Phongsali Province, Laos (Auth 2008)

The perception of bamboo is completely different in western countries where it is viewed as an eco-friendly material and a potential alternative to wood. A modern phenomenon in these countries is the emergence of environmentalism as a symbol of status. Consumers are often willing to pay a premium for products that support sustainability, and bamboo, in the form of flooring and furniture, has become one of those products. The social and cultural value of bamboo manifests as architectural designs that strongly emphasize the native culm form of bamboo, such as in luxury homes by the U.S. based architecture firm Bamboo Living. Design projects by internationally renowned architects like Shoei Yoh, Juvenal Baracco, Simon Velez, and Rocco Yim have also raised the value of bamboo in the high-end architecture market, Figures 3-4.

Figure 3: Temporary Cathedral from Guadua culms in Pereira, Colombia, 1992 designed by architect Simon Velez (Khanna 2009)

Figure 4: Solar powered Passive House with bamboo exterior cladding in Bessancourt, France, 2009 by Karawitz Architecture (ArchDaily 2010)

There is an interesting dichotomy in the perceived value of bamboo in developing countries, where bamboo is native, and the west. On one hand bamboo represents primitiveness and poverty but on the other hand it represents sustainability and environmentalism. At the same time, in developing countries like Brazil, China, and India there is great need for an affordable construction material to address housing shortages in areas of rapid urban development. But it is precisely in this part of the world, where bamboo has such a negative perception.

In traditional bamboo construction, whole bamboo poles are fastened by fish-mouth, rope, plug in, or positive fitting connections to form two dimensional planer frames. These poles are able to withstand compressive and bending stresses. However,

whole bamboo poles must be treated to prevent degradation from insect and microbial digestion and to give fire resistance. Additionally, natural variations in bamboo culms pose a challenge to quality control in construction.

One possible solution is the use of structural bamboo products (SBP). SBPs are formed by breaking down bamboo culms into smaller components and reassembling them to make a composite structure in a manner similar to plywood. SBPs can represent the middle ground between low-income and high-income constructions with bamboo and avoid the negative connotation associated with bamboo because the culm is no longer visible. SBPs also have advantages from a mechanical perspective, since material defects can be removed before reassembly to control for the natural variability in bamboo. SBPs also allow for the formation of larger structural members and are easier to join than the native culm, which opens up new design possibilities.

One structural application of SBPs is as an alternative sheathing material in timber frame construction. Timber frame wall panels are made up of vertical studs and horizontal rails with wood-based panel sheathing and a plasterboard lining. The studs transfer vertical loads to the foundation and sheathing panels are designed as shear walls to resist horizontal loads from wind and seismic forces, a response known as racking resistance. Structural connectors transfer horizontal loads and produce shear forces that are resisted by the joining of the frame, sheathing, and fasteners (Ambrose and Vergun 1999). Nails, screws, stables, and other dowel-type fasteners also dissipate energy. Adequate anchorage and connectors to the foundation, floors, and shear walls resist uplift and sliding. Gravity loads also resist uplift (McCormick 1995). The overall structural

performance is affected by the composite action and stiffness of the shear wall elements and their height and width ratio.

Sheathing panels may be plywood, oriented strand board (OSB), flake boards, gypsum wallboards, or fiberboards. Protective membranes and cladding may be added behind the plasterboard to provide to control internal humidity and provide weather resistance. Thermal insulation, electrical, and plumbing services are also installed within the wall. Bamboo can be used as a substitutive material for vertical studs and panel sheathing.

Another potential structural application is Structural Insulated Panels (SIP), which are composed of two loadbearing layers bonded to a rigid lightweight core. The external face is commonly made of plywood sheets, OSB, fiber-cement boards, or steel and fiber reinforced plastic sheets. The internal layer is usually a polyurethane or polystyrene foam. Agricultural fibers such as wheat straw can also be used to fill the core and can provide insulation and strength (PATH 2006). The core can be either self-bonded or bonded by an adhesive. SIPs can be constructed with or without an internal structural frame. SIPs distribute the acting load homogenously and respond to compression, racking, axial bending, and shear loads as one component. The use of OSB for the external face is widespread. The boards are often plastered with cement to give the medium water proofing and flame resistance and protection from insects and mold. In this case a gypsum dry wall is not needed. A similar result can also be achieved with fiber-cement boards.

Presently the use of bamboo in SIPs is limited by adhesion. Urea-formaldehyde (UF) and phenol-formaldehyde (PF) are commonly used in timber panel construction.

However, these adhesives are not as well suited for bamboo due to differences in the chemical composition and structure. Bamboo has a very low surface wettability, which further hinders good adhesion (Kai and Xuhe 2009).

Figure 5: GluBam concept house in Changsha, Hunan Province, China, 2009 by researchers at the University of Southern California (USC Viterbi School of Engineering News 2009)

There are several examples of small-scale SBP use in construction. Lamboo® WeaveCore, a laminate made of multiple pressed layers of interwoven bamboo slats, was used to create structural insulated panels for the University of Illinois's 2009 Decathlon project (U.S. Department of Energy 2010). GluBam is a composite made by coating strips of bamboo with an adhesive and compressing them into boards and was used in a prototype house in China, Figure 5 (Popular Science 2008). In general the little information available about the manufacture, structural, and thermal properties of SBP limits the use of bamboo in structural applications. Another aspect to consider is the environmental cost of processing bamboo into SBP. Increased processing of bamboo may lead to better mechanical properties of the resulting SBP, but the point of sustainability is defeated if it comes at too great of an environmental cost.

The objective of this study is to characterize the linear and radial variation of the mechanical properties and microstructure of Guadua bamboo (*Guadua angustifolia kunth*). This species is among the largest of the woody bamboos and is widely used in construction in South America. This study also aims to relate the environmental cost of processing of SBP to their mechanical properties as well as compare the environmental cost of SBP to other comparable building materials like wood composites.

Materials and Methods

The structural and mechanical properties of bamboo were evaluated on a section of Guadua bamboo (*Guadua angustifolia kunth*) that had been obtained from Koolbamboo Inc (Miami, FL). According to the supplier, the culm was sourced from Panama and harvested after approximately five years of growth. The culm was then dried and treated with boric acid for protection against insect and fungal attack. The culm was cut through the nodes into six sections that were each approximately 1 m long and had been marked by the supplier so the total culm could be reassembled, Figure 6.

Figure 6: Guadua culm sections as received from Koolbamboo Inc (Miami, FL)

Bamboo Anatomy and Microstructure

The bamboo stem or culm is a hollow cylinder with intermittently distributed solid disks called nodes. Nodes are connected by internodes, where cells are axially oriented. The hollow shape of bamboo gives it a higher moment of inertia than a solid cylinder of the same volume, so bamboo is able to withstand higher forces and moments (Yu 2006). Bamboo is a natural composite material. The inside culm tissue consists of vascular bundles, which are composed of vessels, sieve tubes, companion cells, and sclerenchyma fibers, embedded in a porous matrix of parenchyma cells. Figure 7. The

entire culm is comprised of approximately 50% parenchyma, 40% sclerenchyma fiber, and 10% conducting tissue (vessels and sieves) by volume (Liese 1985). The sclerenchyma fibers run longitudinally through the internodes and are the primary contributor to bamboo's mechanical strength and stiffness, providing structural support to the culm. Sclerenchyma fibers surround vessels and conducting tissue, which are responsible for the transport of water and nutrients.

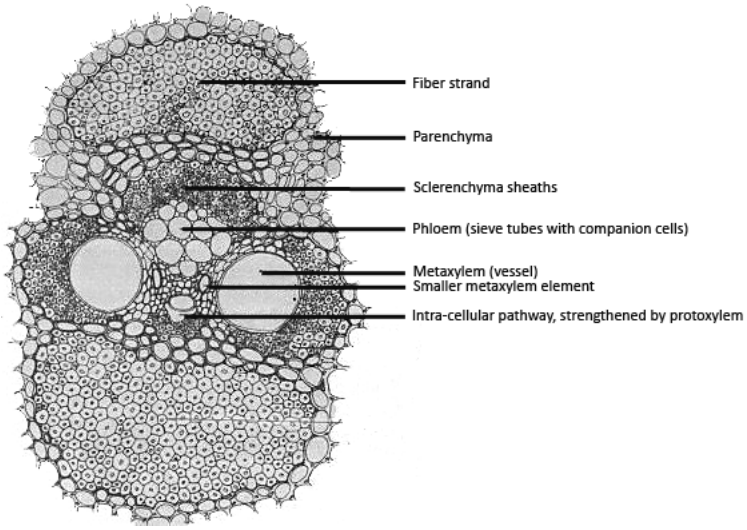

Figure 7: Composiiton of a bamboo vascular bundle (de Vos 2010)

A cross sectional view through an internode reveals the change in density and shape of vascular bundles from the outer to inner wall, Figure 8.

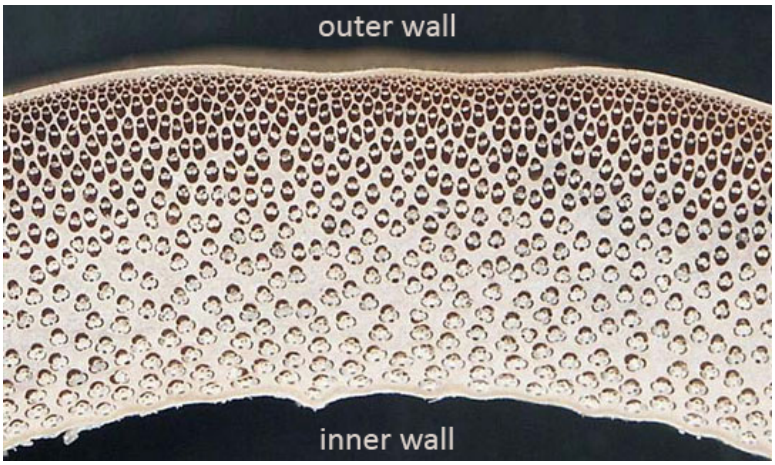

Figure 8: Variation in vascular bundle density and shape through a transverse surface of Guadua bamboo (de Vos 2010)

The outer surface is a cutinized waxy layer called the epidermis or cortex and provides protection from environmental factors. The next zone is characterized by tightly packed small circular vascular bundles with few vessels and conductive tissue in the centers. This is followed by a region of less densely packed vascular bundles with more prominent vessels and conductive tissue in the centers. The innermost layer contains no vascular bundles and composed entirely of parenchyma cells. Part of this study will relate the variation in microstructure to variation in bamboo's mechanical properties.

Nomenclature

Samples for mechanical testing, nanoindentation, and scanning electron microscopy were prepared from internodal sections and labeled in accordance to Figure 9. Nodes and internodes are numbered in order of increasing height beginning with the base of the culm as zero. To correct for varying internodal lengths, the cumulative height at the top of the internode is recorded; this allows us to understand the longitudinal variation of mechanical properties. Samples from the same internode are labeled alphanumerically: A, B, C, etc. To test the positional dependence of macroscopic density and mechanical properties, internodal pieces were split into radial sections as shown in Figure 10. Samples are labeled numerically from the outer (1) to inner (4) wall. To account for varying wall thickness, the radial position is reported as the quotient of the section's distance from the inner wall, r, to the internodal wall thickness before removing the cortex, t.

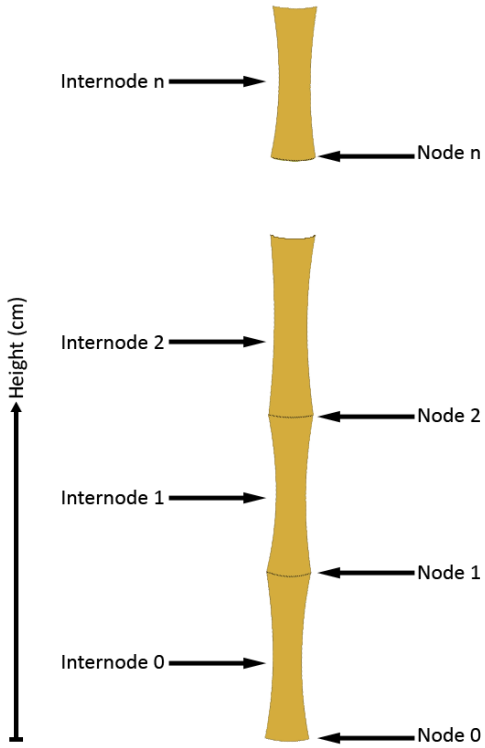

Figure 9: Internode nomenclature

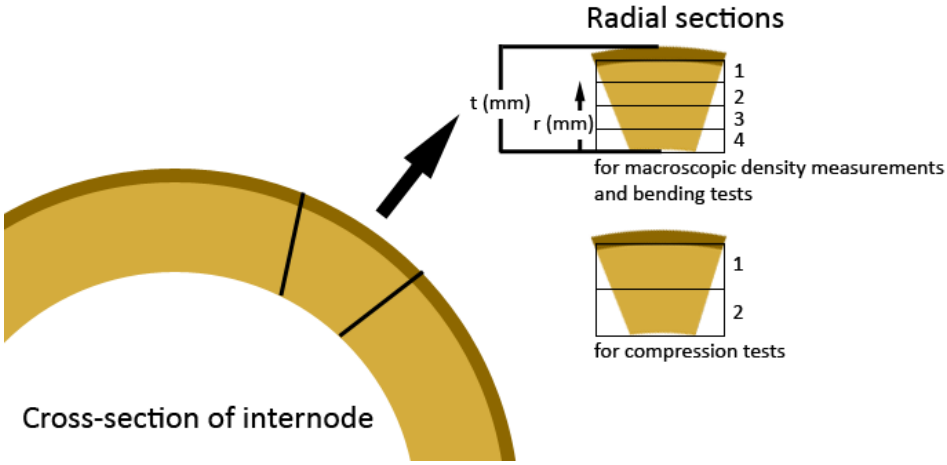

Figure 10: Radial section nomenclature

Scanning Electron Microscopy

Scanning electron microscopy (SEM) was used to image the bamboo surface in order to study the microstructure, Figure 11. Images were taken with a JSM-6610 LV SEM (JEOL, Peobody, MA) at low pressure (30 Pa) using secondary electrons.

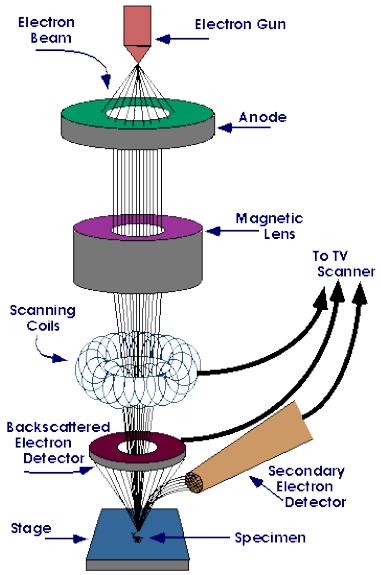

Figure 11: Diagram of scanning electron microscope (SEM) parts and components (Sweitzer n.d.)

SEM samples were prepared by splitting a radial piece from the internode with a hand knife and mallet. A handsaw was used to cut the piece perpendicularly to a length of approximately 15 mm. Cut samples were soaked overnight in deionized water to soften surface tissues. Samples were then polished according to Stuers method 368 on a Stuers Rotopol-1 polishing wheel with six different Si-C papers of decreasing particle grain size: 200 grit, 500 grit, 800 grit, 1200 grit, 2400 grit, and 4000 grit. A stainless steel jig was used to support the bamboo piece while polishing so that the top and bottom surface remain parallel after the 200 grit Si-C paper. Samples were not polished in a single direction for more than four minutes in order to avoid scratching the surface. Samples were left to dry for at least two days before placing inside of the SEM, which ensures the

microstructure returns to its dry state. While polishing the surface does fill parenchyma pores with material removed during polishing, which makes it difficult to analyze pore size and shape, dried Guadua bamboo was too tough to slice evenly with a hand knife.

SEM images were stitched together using the panorama tool in Adobe Photoshop Elements 6 (Adobe, San Jose, CA) to show the microstructure across the entire wall thickness of the internode. Also in Photoshop Elements 6, sclerenchyma sheaths were selected automatically with the Magic Wand tool and manually with the Magnetic Lasso tool and filled black, giving a binary image. The cross section was split into radial sections that were 1 mm^2 and was processed with the Analyze Particles function in ImageJ (NIH, Bethesda, MD), which returns the area of each sclerenchyma sheath in that radial section. The area fraction per radial section was found by dividing the cumulative particle area by $1mm^2$.

Compression tests

It was not possible to do full ring compression tests as the dried Guadua bamboo had cracks. Compression samples were prepared by splitting a radial piece from the internode of the same width as the intermodal wall thickness with a knife and mallet. The cortex was removed with a belt sander. A handsaw was used to cut the piece perpendicularly to a length also equal to the wall thickness. The bamboo cube was split in half with a knife and mallet to give an inner and outer radial section. Sample dimensions were measured with calipers in order to calculate the cross-sectional surface area and volume and are provided in the Appendix. The mass of each sample was measured using a Cole-Parmer Symmetry ECII balance (Cole Parmer, Vernon Hills, IL) and used to calculate the density.

Samples were compressed at a rate of 1 mm/min in an Instron 1321 frame controlled by a model 8500 Plus controller (Instron, Norwood, MA). The load and displacement were measured using the Instron's load cell. Initial runs were conducted using a fixed compression plates, but after observing failure due to brooming, the top plate was replaced with a variable tilt compression plate. While using the fixed compression plate the load was measured using the Instron's load cell and displacement was measured using a direct-current linear variable differential transformer (LVDT) model 0243-0000 (Trans-Tek Inc., Elington, CT) connected to a DC power supply (Hewlett-Packard model E3612A, Palo Alto, CA) and outputting at approximately 15 V. With the tilted plate the load and displacement were both measured using the Instron's load cell. The load and displacement were recorded using a National Instruments data acquisition module (NI USB-6211) and LabView software (National Instruments, Austin, TX). The acquired load and displacement data was processed in MATLAB (MathWorks, Natick, MA) and transformed to stress and strain respectively by using the measured sample dimensions and Equations 1 and 2 respectively. The plot of stress versus strain was used to determine the modulus of elasticity (MOE), Equation 3, and the compressive strength. The compressive strength was recorded as either the intersection of the elastic regime and plastic regime of the stress-strain curve or the maximum stress, see Results and Discussion.

$$\sigma = \frac{P}{A} \tag{1}$$

Where σ is the stress, P is the load, and A is the cross sectional area

$$\varepsilon = \frac{\delta}{l_0} \tag{2}$$

Where ε is the strain, δ is the displacement, and l_0 is the initial sample length

$$E = \frac{\sigma}{\varepsilon} \tag{3}$$

Where E is the MOE, σ is the stress, and ε is the strain

Tension and bending tests

Samples for tension tests were prepared by splitting a radial piece approximately 15 mm wide and 115 mm long from the internode with a knife and mallet. The cortex was removed with a belt sander. The bamboo piece was then split into four sections by first splitting the piece in half and then splitting each half into half again using a knife and mallet. Sample dimensions were measured with calipers to calculate the volume. The mass of each sample was measured using a Cole-Parmer Symmetry ECII balance (Cole Parmer, Vernon Hills, IL) to calculate the density. Dog bones in the shape of the template shown in Figure 12 were cut out using an OMAX 2626 JetMachining Center waterjet (Omax, Kent, WA)

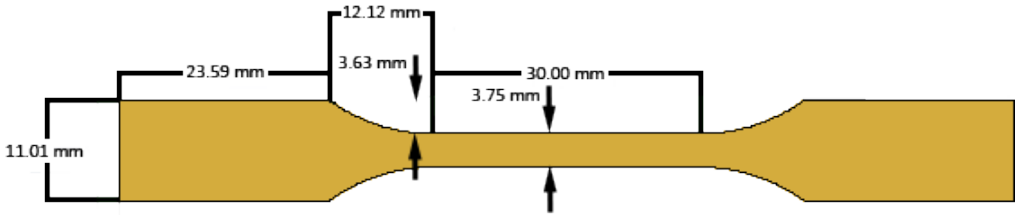

Figure 12: Shape and dimensions of dogbone template for tensile testing

Samples were dried overnight before conducting tension tests in an Instron Model 4206. A static extensometer (model number 2630-104. Instron, Norwood, MA) was used to measure strain. A strain rate of 1 mm/min was used and samples were tested to failure. The load and displacement were recorded using a National Instruments data acquisition module (NI USB-6211) and LabView software (National Instruments, Austin, TX). In

initial runs, tensile failure occurred in the grips and not the gauge length, suggesting a high stress concentration at the grips. Modifications such as increasing the grip size and thickness and mounting the dog bone grips in epoxy did not consistently give tensile failure in the gauge length. Tensile samples were modified for bending tests by cutting off the grips with a knife and sanded with Si-C paper, Figure 13.

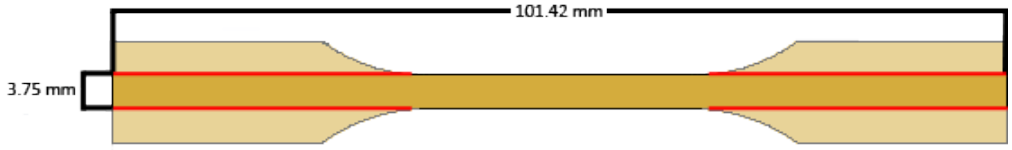

Figure 13: Shape and dimensions of beam for bending tests relative to the original tensile dog bone. Knife cuts were made along red lines.

With the modified tensile samples, 3-point bending tests were conducted with a support span of 86.49 mm using an Instron Model 4206 and static extensometer model number 2630-104 (Instron, Norwood, MA). The load was measured using the Instron's load cell, while displacement was measured using a direct-current linear variable differential transformer (LVDT) model 0243-0000 (Trans-Tek Inc., Elington, CT) connected to a DC power supply (Hewlett-Packard model E3612A, Palo Alto, CA) and outputting at approximately 15 V. The load and displacement were recorded using a National Instruments data acquisition module (NI USB-6211) and LabView software (National Instruments, Austin, TX). The acquired load and displacement data was processed in MATLAB (MathWorks, Natick, MA) and used to calculate MOE, Equation 4, and modulus of rupture (MOR), Equation 5.

$$E = \frac{\left(P/\delta\right)l^3}{48I} \tag{4}$$

Where E is the MOE, P is the load, δ is the deflection, l is the span length, and I is the moment of inertia

$$\sigma_{MOR} = \frac{3}{2}\frac{P_{max}l}{bd^2} \quad (5)$$

Where σ_{MOR} is the MOR, P_{max} is the maximum load, l is the span length, b is the width, and d is the thickness

Nanoindentation

Nanoindentation samples were prepared by splitting a radial piece about 5 mm wide from the internode with a hand knife and mallet. A handsaw was used to cut the piece perpendicularly to a length of approximately 25 mm. Several bamboo pieces were mounted on EpoFix in a 1-inch diameter silicone mold. The pour epoxy did not exceed 0.5 inch in the mold with the bamboo samples and was allowed to dry for at least fourteen hours. Excess bamboo material above the epoxy puck was cut with a handsaw. Samples were then polished according to Stuers method 368 on a Stuers Rotopol-1 polishing wheel. Samples are sanded with six different Si-C papers of decreasing particle grain size 200 grit, 500 grit, 800 grit, 1200 grit, 2400 grit, and 4000 grit. A stainless steel jig was designed to support the epoxy-mounted samples while polishing so that the top and bottom surface remain parallel and was used after the 200 grit Si-C paper. Samples were not polished in a single direction for more than four minutes in order to avoid scratching the surface.

Nanoindentation of the vascular bundles was performed using a diamond Berkovich tip on a Hysitron tribodenter to obtain the local hardness and modulus of elasticity. The machine was calibrated by first indenting a fused silica sample of known mechanical properties. The prepared samples were indented along the bamboo fiber direction. Indentation areas were selected in situ using the optical microscope embedded into the Hysitorn tribodenter to select for areas that were free of scratches and away from

the porous matrix. Each indentation area contained twenty-five indents in a five by five grid with 5-μm spacing between indents. The load function used for nanoindentation is shown in Figure 14 and is a modification from that used in prior bamboo nanoindentation experiments (Yu 2006). A load and unload rate of 50 μN/s to a peak load of 500 μN with a hold time of 5 s between loading and unloading was used. This load function produced analyzable results for Moso bamboo (*Phyllostachys edulis*) and was used to maintain consistency of results.

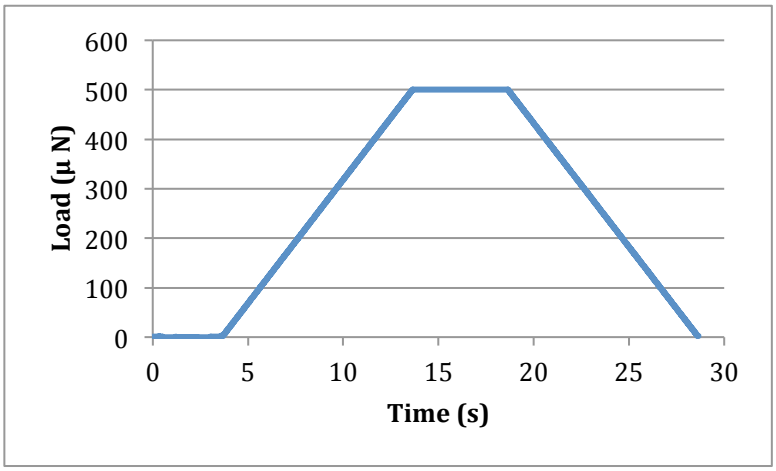

Figure 14: Load function for nanoindentation experiments

The unloading section of the resulting load-displacement curve was analyzed using the Oliver-Pharr method to give the reduced elastic modulus and hardness. The reduced elastic modulus is a function of the mechanical properties of the indenter tip and the sample, Equation 6.

$$\frac{1}{E_r} = \frac{1 - v_i^2}{E_i} + \frac{1 - v_s^2}{E_s} \quad (6)$$

Where $\mathbf{E_r}$ is the reduced MOE, $\mathbf{E_i}$ is the MOE of the indenter tip, $\mathbf{E_s}$ is the MOE of the sample, $\boldsymbol{\nu_i}$ is the Poisson's ratio of the indenter tip, and $\boldsymbol{\nu_s}$ is the Poisson's ratio of the sample

The hardness is calculated from Equation 7.

$$H = \frac{P_{max}}{A(h_c)} \quad (7)$$

Where **H** is the hardness, $\mathbf{P_{max}}$ is the maximum load, and **A** is the indentation area, which is a of the contact depth, $\mathbf{h_c}$

The properties of the indenter tip are known and the reduced elastic modulus is measured. A Poisson's ratio for the bamboo of 0.38 was used, based on the literature (Wan and Ko 2011). The Poisson's ratio for the diamond indenter tip is 0.07 and the indenter elastic modulus is 1140 GPa.

Results and Discussion

Macrostructure

The internodal length and wall thickness as a function of internode number are shown in Figure 15. From internode 1 to 24 the internodal length increases linearly from 13 cm to 38 cm. Internode 25 is an anomaly, with a length of 18 cm, which suggests that the top section of the culm received was removed. The internodal length is greatest at the midpoint of the culm (Amada, et al. 1997). This implies that all of the internodes in this Guadua section are from the lower half of the culm. The wall thickness decreases monotonically with increasing internode number, which is consistent with other bamboo species (Garcia 2011)

In comparison to sweetshoot bamboo (*Phyllostachys dulcis*) and Japanese timber bamboo (*Phyllostachys bambusoides*), mature Guadua culms are much taller and have internodal wall thicknesses that are at least twice as large as the other species. (Garcia 2011). In Moso bamboo (Phyllostachys edulis), the maximum internodal length of 30 cm was attained at an internodal number near 25 (Amada, et al. 1997). Based on the trend in Figure 15 (a), mature Guadua culms are also taller than Moso bamboo. While lower internodes of Moso have similar wall thicknesses to that of Guadua, the rate of decreasing wall thickness with height was higher for Moso. Both species had lower internode wall thicknesses of approximately 20 mm, but in Moso the wall thickness decreased to 10 mm at an internodal number of 12, while a similar decrease in Guadua occurred at an internodal number of 25 (Amada, et al. 1997).

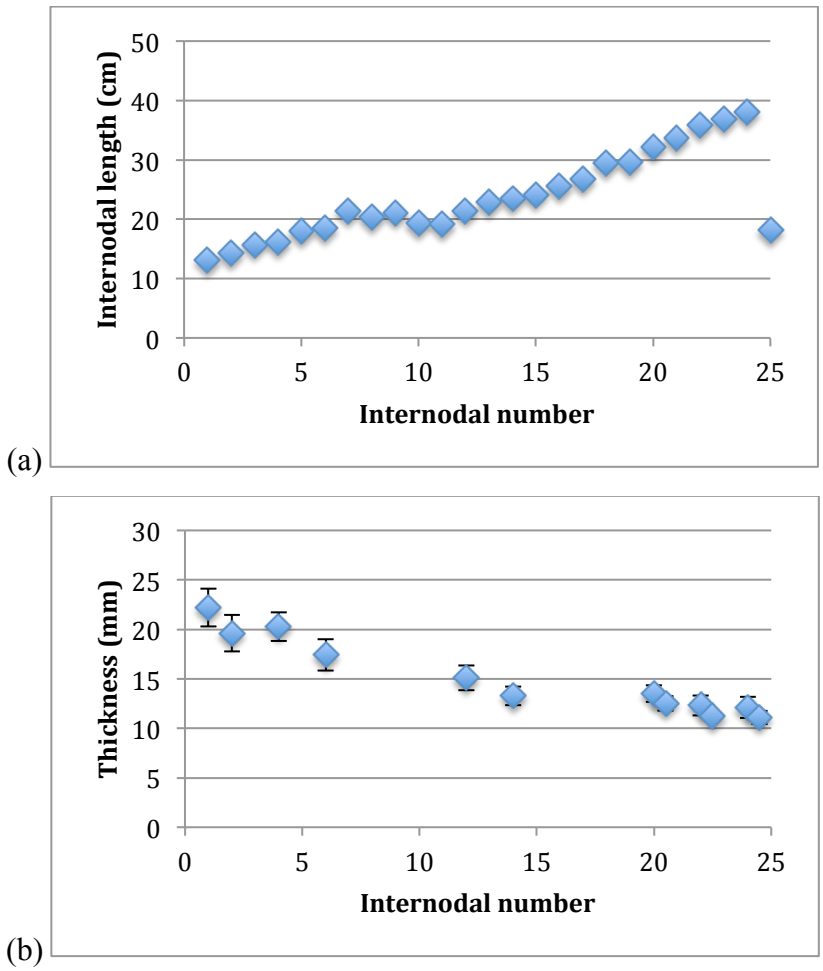

Figure 15: Variation in intermodal length and wall thickness as a function of intermodal number for the Guadua culm section

Macroscopic density was measured from four radial sections prior to cutting dog bones for tensile testing. The density as a function of internodal height and radial position are shown in Figures 16-17.

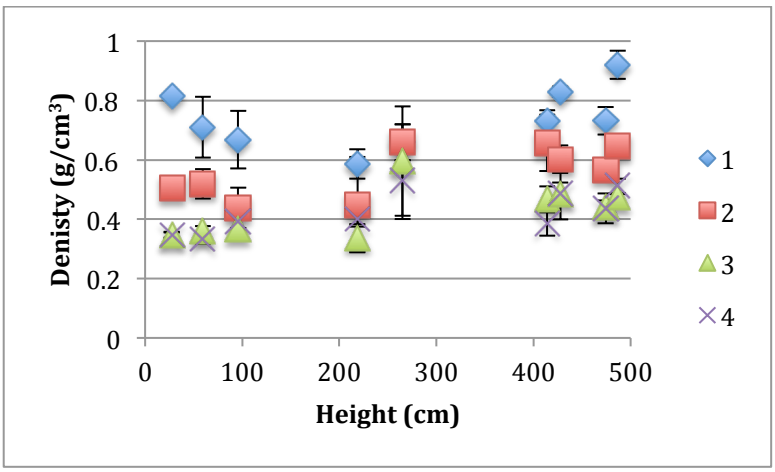

Figure 16: Density with respect to height for four radial sections

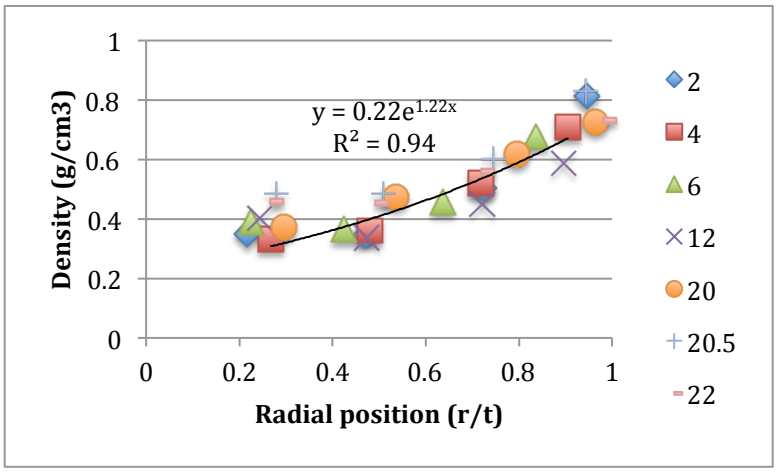

Figure 17: Density versus radial position for seven heights along the culm

With respect to height, density does not vary significantly for each of the four radial sections. In contrast, for other bamboo species a logarithmic variation for the area fraction with respect to height is reported (Garcia 2011). Another study of Moso bamboo found that the density increased with height (Nogata and Takahashi 1995). In this study all comprise of the lower half of the Guadua culm, which may explain why density is not a function of height along the culm.

The density increases exponentially with respect to the radial position from 0.4 g/cm^3 to 0.8 g/cm^3. The exponential relationship between density and radial position is consistent with that for other bamboo species (Nogata and Takahashi 1995). In

comparison to Sweetshoot bamboo, whose density ranged from 0.7 g/cm^3 to 0.9 g/cm^3, the Guadua internode appears to have greater variation in density with radial position (Garcia 2011). However, the Sweetshoot specimen represents a fresh bamboo, so the narrow density range may be due to higher moisture content.

Microstructure

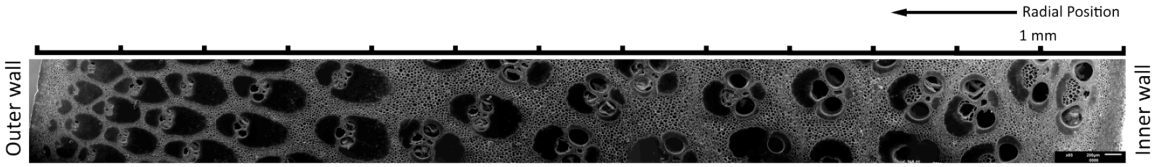

Figure 18: Variation in vascular bundle density and shape through a transverse cross section of Guadua

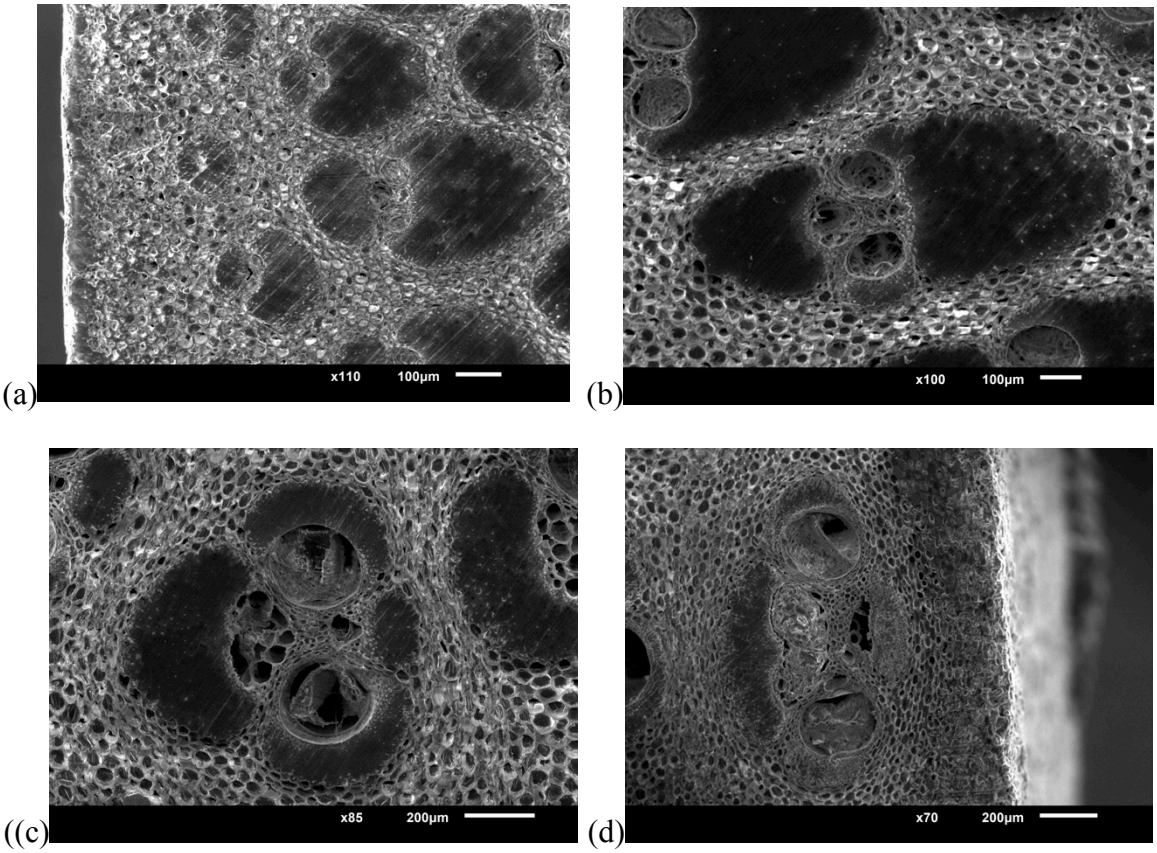

Figure 19: Variation in vascular bundle shape and area of sclerenchyma at radial positions (r/t) of approximately 0.75 (a), 0.57 (b), 0.17 (c), and 0.06 (d)

The bamboo microstructure varies with radial position, Figures 18-19. The outer wall is comprised of small close backed fiber sheath with no vessels or conducting tissue.

Moving towards the inner wall, the vascular bundles become more elliptical in shape and have small vessels and conducting tissue. Continuing to move towards the inner wall, vascular bundles return to a rounder shape, with three large vessels. At the inner wall, vascular bundle size decreases.

Related to the vascular bundle shape and size, the area fraction of sclerenchyma fiber varies with radial position. The area fraction of sclerenchyma sheaths was measured for three internodes and is plotted in Figure 20. The results show the fiber area fraction does not vary significantly with height, but increases monotonically with radial position.

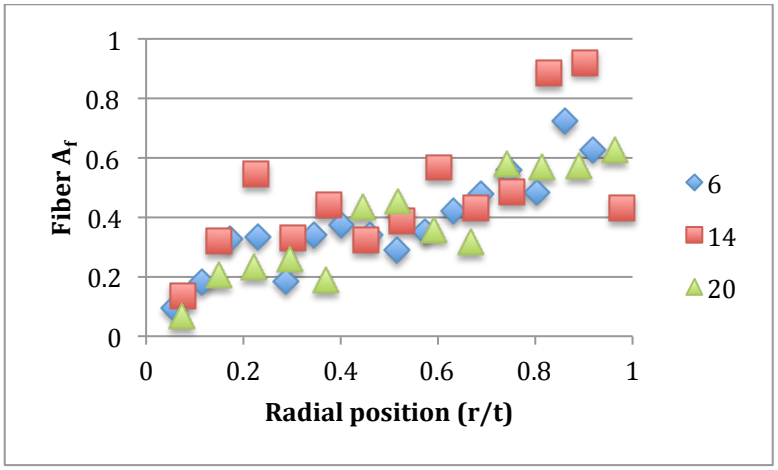

Figure 20: Sclernchyma area fraction as a function of radial position for three internodal numbers

The fiber area fraction will be related to the macroscopic density measured for different radial positions and the results are shown in Figure 21 for the three internodes. For all three internodes, the macroscopic density correlates directly with the fiber area fraction. This means that mechanical properties of bamboo that are a function of macroscopic density also relate to the area fraction of sclerenchyma fibers.

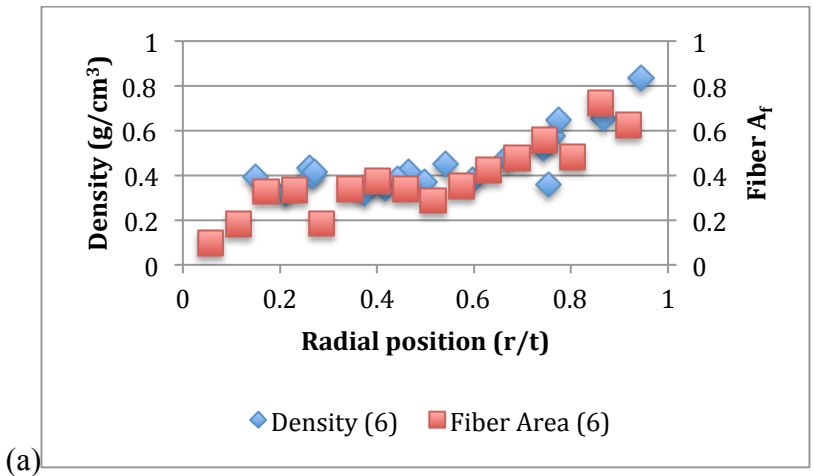

(a)

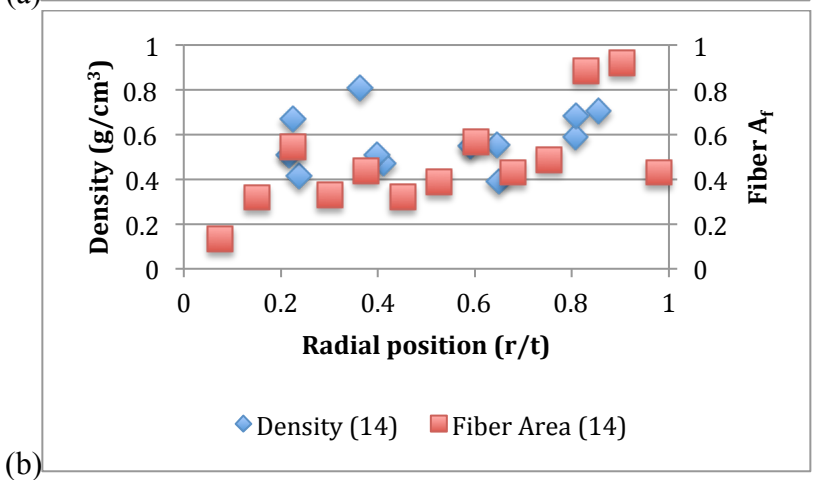

(b)

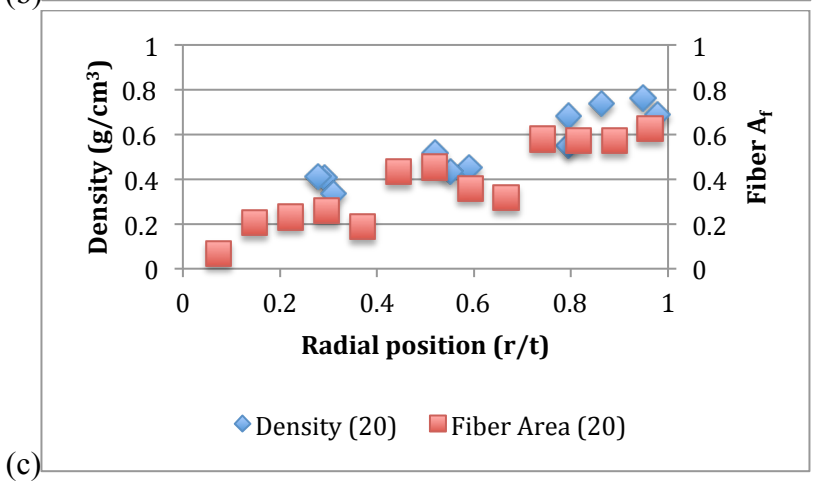

(c)

Figure 21: Macroscopic density and sclerenchyma area fraction with respect to radial position for three internodes: 6 (a), 14 (b), and 20 (c)

Compressive properties

The plot of stress versus strains shows that bamboo compression behavior is characterized by a period of linear deformation followed by yielding before failure. The Young's modulus and compressive strength were measured for samples prepared from seven different heights along the culm and two radial sections at each height. Initially a fixed compression plate was used, but failure by brooming was observed, which is associated with reduced load. Comparing multiple samples from each plate type, there was significantly more variation in the maximum stress for samples measured using the fixed plate than the tilted plate, Figures 22-23. For this reason, further tests utilized the tilted plate in order to obtain a more consistent value for the compressive strength. With the tilted plate the modes of failure observed were shear, splitting, or a combination of both. Even with the tilted compression plate, some brooming was still observed, so the reported results may be an underestimate of the compressive strength.

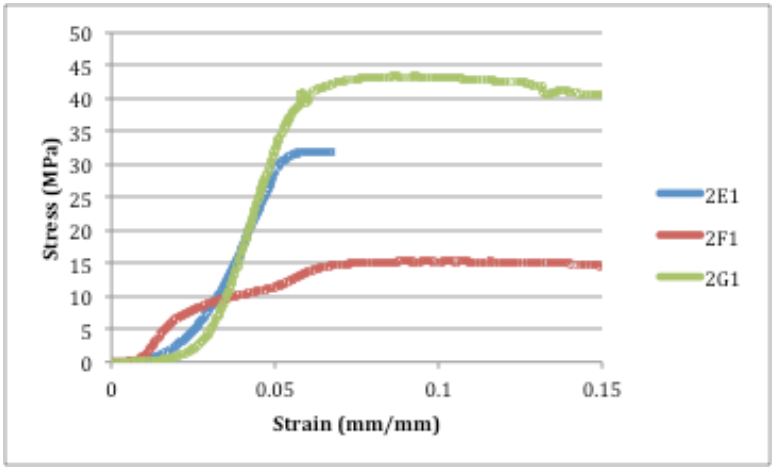

Figure 22: Stress-strain curves for compression testing with fixed compression plates for outer radial section samples from internode 2 with an average density of 0.65 g/cm^3 shows large variation in maximum stress

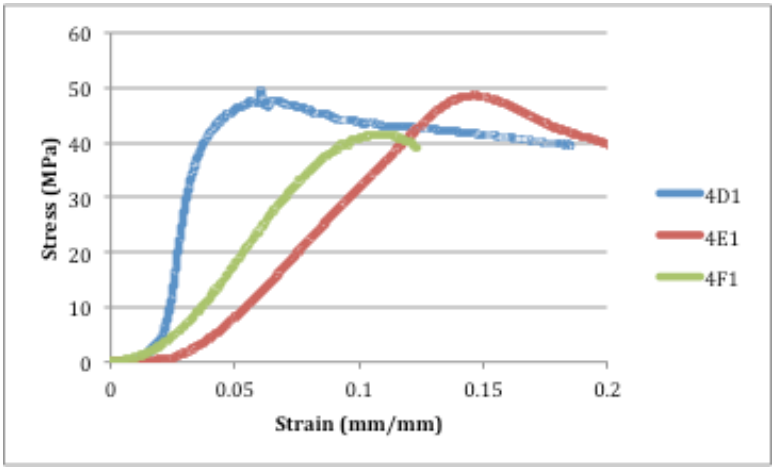

Figure 23: Stress-strain curves for compression testing with tilted compression top plate for outer radial sections from internode 4 with an average density of 0.68 g/cm^3 shows consistency in the measured maximum stress

(a) (b) (c)

Figure 24: Observed modes of failure in compression- brooming (a), shear (b), and splitting (c)

The stress-strain curves for all samples are available in the Appendix. The MOE was calculated from the slope of the linear region of the stress-strain curve and is plotted with respect to the density in Figure 25.

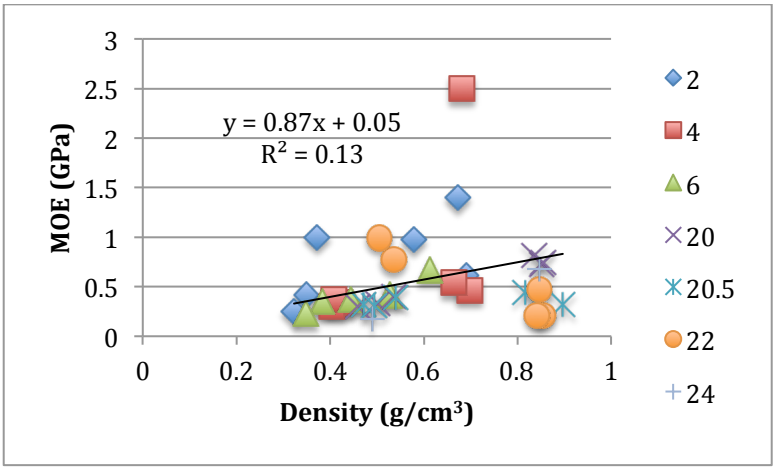

Figure 25: MOE with respect to macroscopic density from compression test results

The MOE measured from compression ranged from 0.25 GPa to 2.5 GPa. There is a very weak linear relationship between the MOE and density. In comparison, full ring compression tests yielded MOE that ranged from 0.3 GPa to 7.2 GPa (Gerhardt 2012). The MOE of Guadua with a density of 0.6 g/cm^3 is reported as 14 GPa (de Vos 2010). The discrepancy in the measured MOE could arise from local uneven crushing at the specimen's surfaces in direct contact with the plates. The strain is measured over the whole body length and due to the small size of the sample, edge effects and internal displacement can have a significant effect on measurements. There may also be effects from misalignment from the tilted compression plate complicating the strain in the specimen.

The compressive strength was determined by finding the intersection between the linear elastic region and the plastic region of the stress strain curve. However, for samples using the tilted compression plate, Figure 23, the plastic region was more parabolic than linear. For these samples the reported compressive strength is the maximum stress.

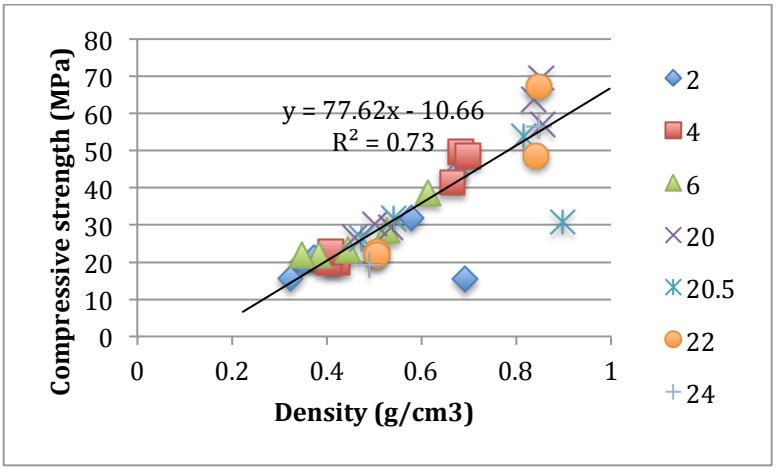

Figure 26: Compressive strength with respect to macroscopic density

Figure 26 shows that there is a linear correlation between the compressive strength and the density. Full ring compression tests of Moso bamboo also showed a linear relationship between the compressive strength and density (Gerhardt 2012). For similar densities, the reported compressive strength for Moso was higher than that measured for Guadua. For a density of 0.5 g/cm^3 the compressive strength of Moso was 40 MPa while that for Guadua was 28 MPa. Similarly for a density of 0.8 g/cm^3 the compressive strength of Moso was 96 MPa while that of Guadua was 70 MPa (Gerhardt 2012). This may either be a difference between the two bamboo species of the result of a reduced load due to failure in brooming.

The results from Figure 26 can also be used to extrapolate the compressive strength of pure bamboo fibers. Single bamboo fiber tests of *Guadua angustfolia* found a fiber density of 1.4 g/cm^3 (Trujillo, et al. 2012). Extrapolating from line of best fit in Figure 26 suggests that the compressive strength of pure bamboo fiber is 98 MPa.

Tensile properties

Figure 27 shows typical plots of stress versus strain for several tensile specimens. All specimens failed in the grips, which indicates a high stress concentration at the grips.

A similar issue was observed for the outer radial sections of Moso bamboo. Increasing the grip size and taper between the grip and the gauge did not lead to consistent gauge failure in the Moso bamboo, so it was not tested in Guadua. Presently a method where dog bone grips are mounted in epoxy is being tested in Moso and can be applied to Guadua if successful.

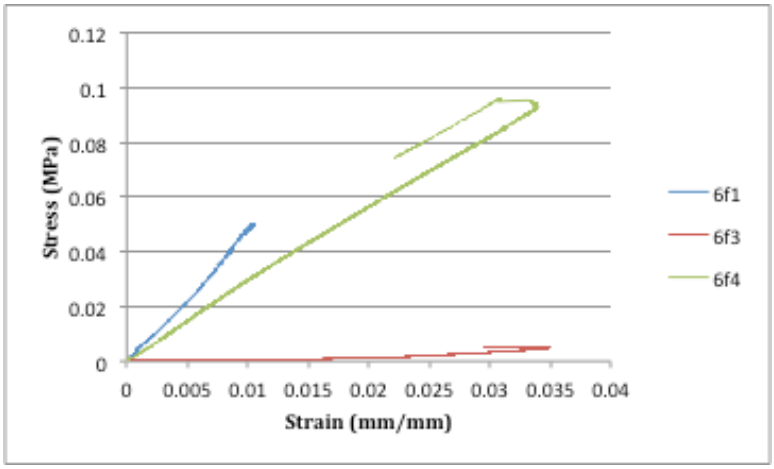

Figure 27: Plot of stress versus strain from tensile test of three radial sections of internode 6. All specimens failed at the dog bone grip

Figure 28 shows four radial sections from the second internode after 3-point bending tests. The plot of load versus displacement, Figure 29, was used to calculate the MOE and the MOR for four radial sections from three internode heights. The plot also shows that bamboo tension behavior is characterized by a period of linear deformation followed by yielding before fracture.

Figures 30-31 summarize the MOE and MOR with respect to the radial position for each internodal height. Both the MOE and MOR increase exponentially with the radial position and do not vary significantly for the three internodal heights. Figures 32-33 show the MOE and MOR versus density. Both the MOE and MOR are linear with respect to density, as would be predicted by the rule of mixtures for a two phase composite. Again, the MOE and MOR do not vary significantly with height.

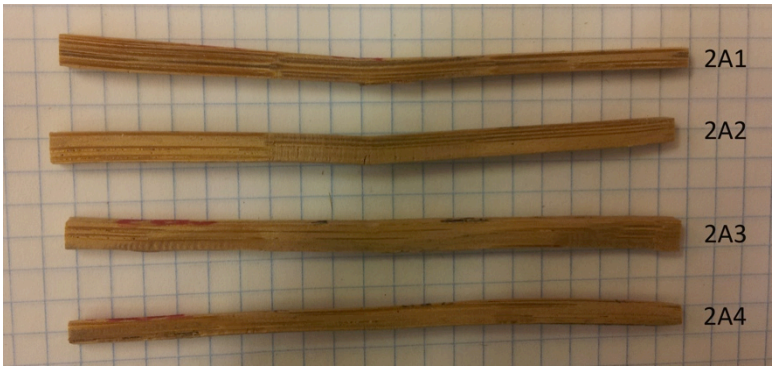

Figure 28: Bending samples for four radial sections of the second internode after 3-point bending

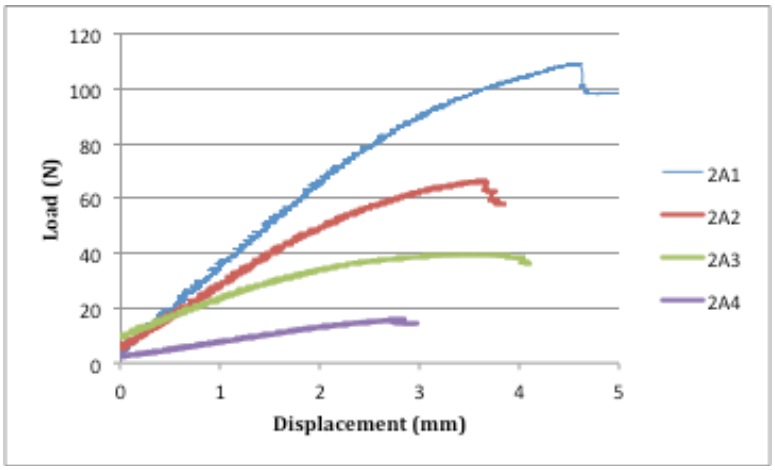

Figure 29: Plot of load versus displacement from 3-point bending tests for four radial sections in the second internode

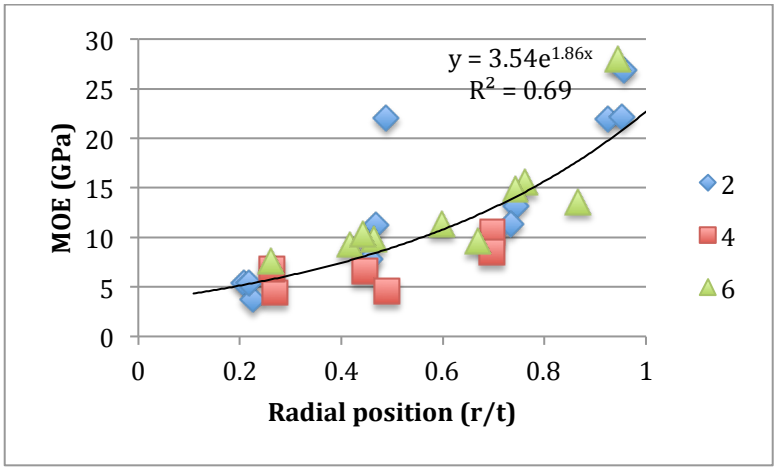

Figure 30: MOE versus radial position from bending tests

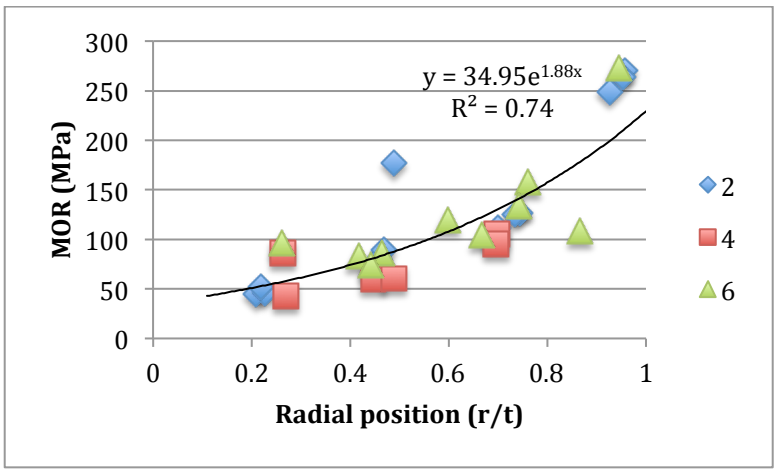

Figure 31: MOR versus radial position for bending tests

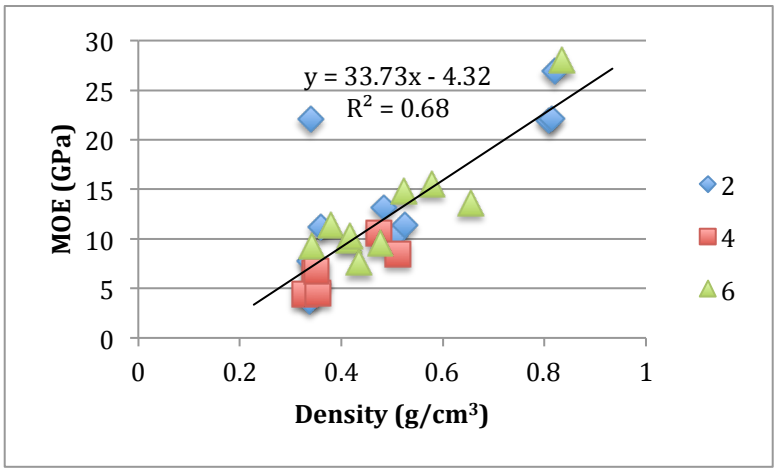

Figure 32: MOE versus macroscopic density for bending tests

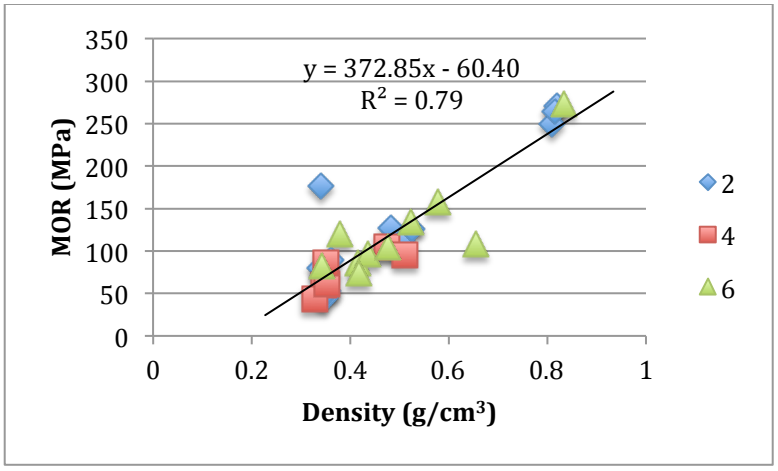

Figure 33: MOR versus macroscopic density for bending tests

The measured MOE increased from 4 GPa to 28 GPa, a factor of seven, which is a similar increase as what was reported for Moso bamboo (Garcia 2011).

Figures 32-33 can be used to extrapolate the mechanical values of pure bamboo fiber as was done for the compressive strength. Assuming a bamboo fiber density of 1.4 g/cm^3, the estimated MOE of pure bamboo fiber is 42 GPa This value is less than an MOE calculated from the rule of mixtures of 55 GPa but within error of an experimentally measured MOE of pure bamboo fiber (Nogata and Takahashi 1995) (Trujillo, et al. 2012).

Nanoindentation

The mechanical properties of the sclerenchyma fibers were evaluated through nanoindentation. Figure 34 shows the force-depth curve for the outer section of the fourth internode. During loading, the force increases exponentially with depth. During a hold time of 5 seconds, the load is constant. At a peak force of 500 μN, the depth is 150 nm. The unloading curve is used to quantify the elastic behavior of the bamboo fiber and the peak load is used to calculate the hardness.

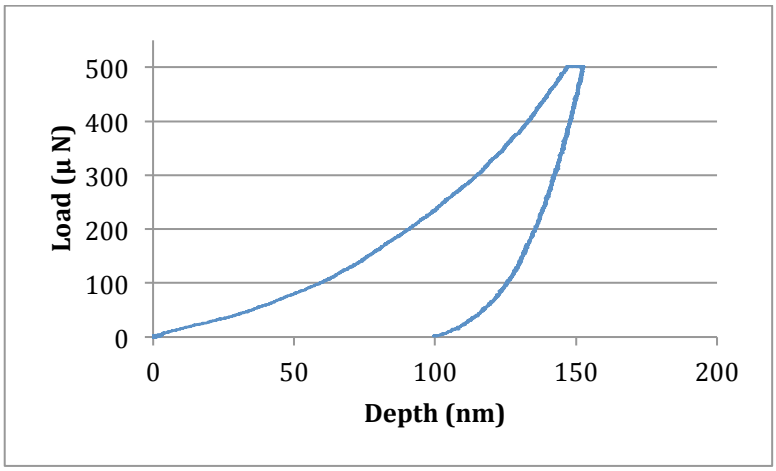

Figure 34: The force-depth curve near the outer wall of the fourth internode

The reduced elastic modulus and hardness of the sclerenchyma fibers are reported with respect to height and radial position in Figures 35-36. The results show that sclerenchyma fiber modulus and hardness does not vary significantly with position. This

simplifies modeling of bamboo, as the properties of the solid can be assumed constant and not dependent on position.

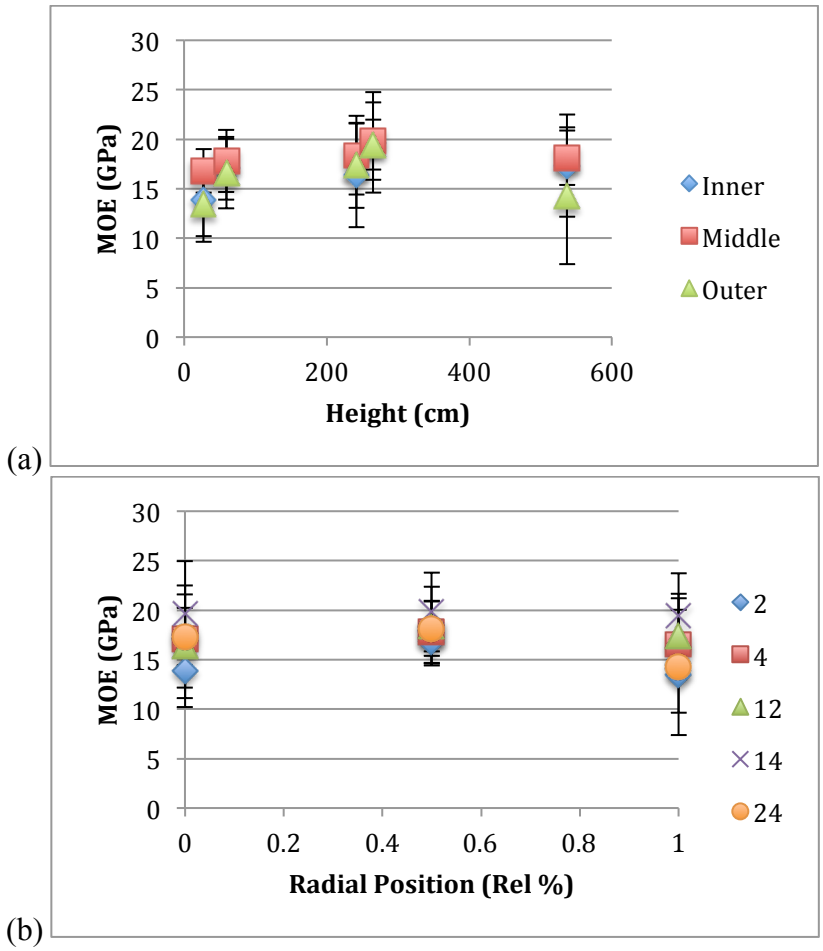

Figure 35: The reduced elastic modulus with respect to height (a) and radial position (b)

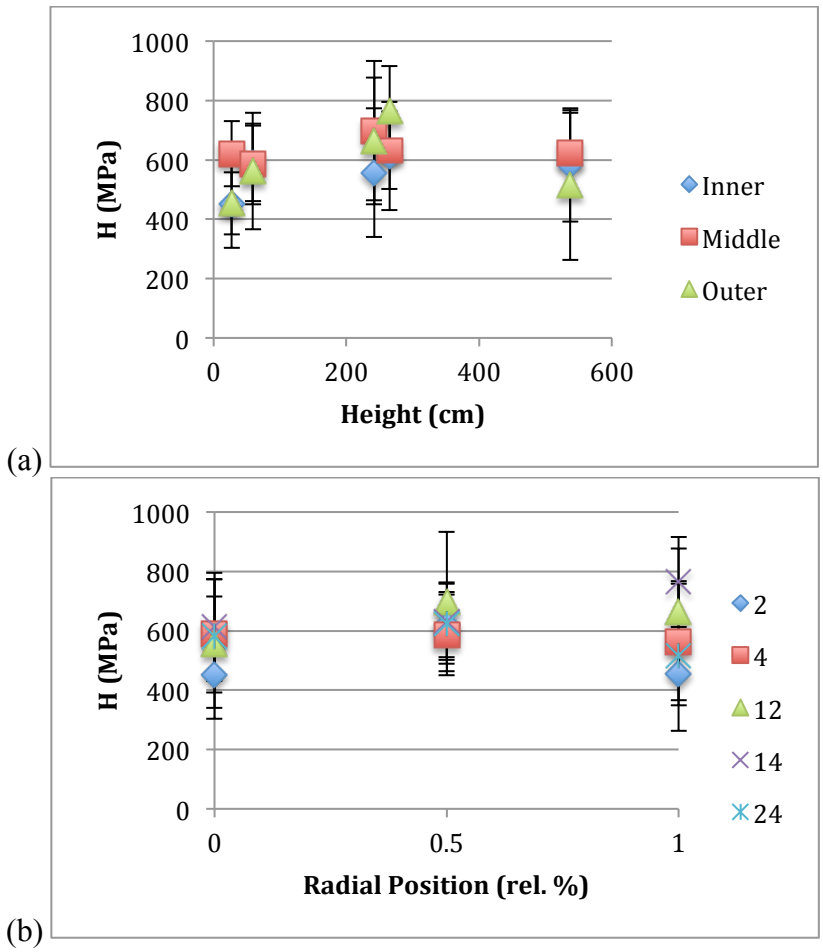

Figure 36: The hardness with respect to height (a) and radial position (b)

Overall, the Young's modulus ranged from 13 to 19 GPa, with an average value of 17 GPa. Nanoindentation experiments of Moso bamboo (*Phyllostachys edulis*) by Yu et al. found the elastic modulus to range from 11 to 26 GPa, with an average of 16 GPa, suggesting that Guadua has a similar stiffness to Moso.

In comparison to extrapolated values for the MOE of pure bamboo fiber from the results from bending, the nanonindention results are off by a factor of two. The Oliver-Pharr analysis used to obtain the reduced elastic modulus assumes an isotropic material, which bamboo is not. Bamboo fibers are stiffer in the longitudinal direction and significantly less stiff in the perpendicular direction (Yu 2006). The measured reduced modulus is a function of the material stiffness in all directions.

Environmental Feasibility

As discussed in the Introduction, bamboo can be utilized in construction in the raw culm form or as a SBP. Process steps for a cradle-to-gate environmental assessments of raw culm and glue pressed bamboo composite, a type of SBP, are presented in Figures 37-38.

Review of studies on the production of glue pressed bamboo boards found most variation in how bamboo strips and layers were pressed. The purpose of the pressing step is to exert pressure on the board in order to accelerate bonding between strips and/or layers of bamboo and adhesive. Pressing can take place in the absence or presence of heat, cold-press and hot-press respectively. Furthermore pressure can be exerted without electricity (low-tech) such as using a heavy weight or bolting layers in a jig, or with electricity (high-tech) such as by hydraulics or pneumatics. From the literature review, three common pressing methodologies, categorized as low-tech cold press, high-tech cold press, and high-tech hot press were identified. Each of these pressing stages has a different energy input requirement, which will lead to a different overall carbon footprint for bamboo composite production. Additionally the pressing methodology affects the degree of bonding between bamboo layers and strips, which has a consequence on the composite's overall mechanical properties.

The environmental feasibility component of this study aims to answer the questions of:

- Is there is a mechanical advantage to processing bamboo into a composite in comparison to raw bamboo?
- Is there is a relationship between the environmental impact of the construction material and its mechanical properties?

- How bamboo composites compare to wood composites used for similar applications?

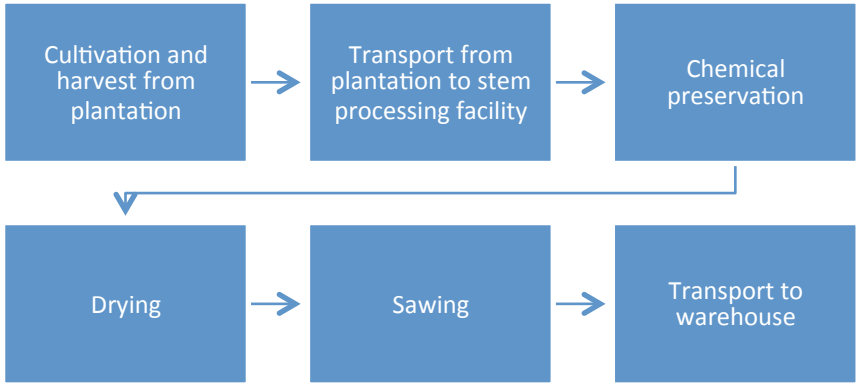

Figure 37: Process steps for a cradle-to-gate environmental assessment of raw bamboo culms

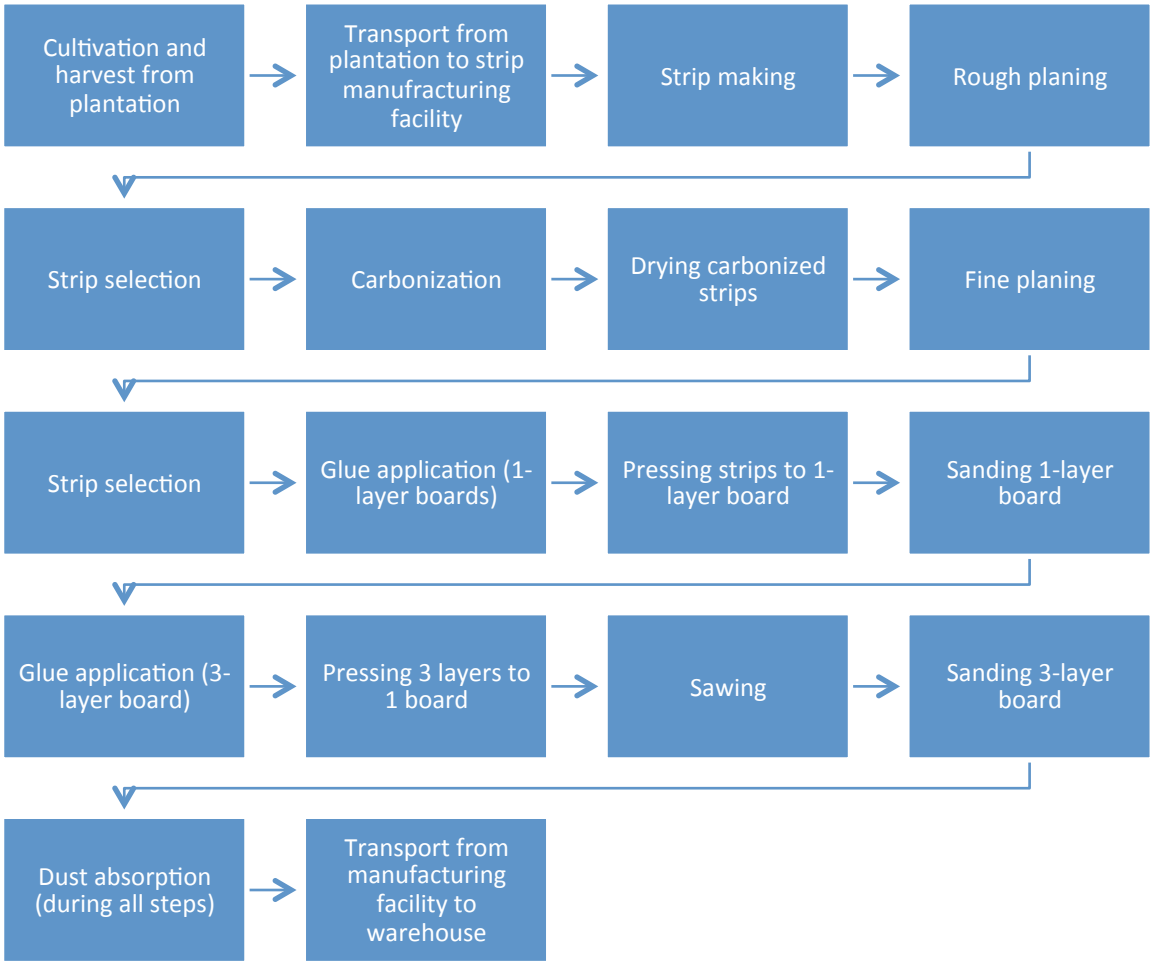

Figure 38: Process steps for a cradle-to-gate environmental assessment of 3-ply glue pressed bamboo board (van der Lugt, Vogtlander and Brezet 2012)

The environmental impact of utilizing bamboo in either form can be analyzed in terms of depletion of resources, deterioration of ecosystems, and/or deterioration of human health. This study will focus on the impact of depletion of resources, specifically from the exhaustion of energy. The process steps listed in Figures 37-38 show that the energy inputs are in the form of gasoline during transportation or electricity from the local grid during cutting and manufacturing. The ecological cost from transport depends on where the bamboo is processed and utilized relative to where it is cultivated. In order to normalize SBP to other wood composites, the ecological cost of transportation was excluded and instead the electricity consumption is compared. The functional unit is the size of a standard plywood sheath panel: 1.2 m x 2.4 m x 20 mm.

Table 1: Process steps where electricity is consumed for different pressing methods

	Low-tech cold press	High-tech hot and cold press
1. Strip making	✓	✓
2. Rough planing	✓	✓
3. Strip selection	✓	✓
4. Fine planing	✓	✓
5. Drying carbonized strips	✓	✓
6. Carbonization	✓	✓
7. Strip selection	✓	✓
8. Glue application (1-layer boards)	✓	✓
9. Pressing strips to 1-layer board	-	✓
10. Sanding 1-layer board	✓	✓
11. Glue application (3-layer board)	✓	✓
12. Pressing 3 layers to 1 board	-	✓
13. Sawing	✓	✓
14. Sanding 3-layer board	✓	✓
15. Dust absorption (during all steps)	✓	✓

Table 1 summarizes the process steps where electricity is consumed for each pressing method for glue pressed bamboo composites. Steps 9 and 12 involve pressing, and the electricity consumed varies depending on the pressing method. The electricity

consumption for all other steps is assumed to be the same regardless of the pressing method, and the values for these steps and the electricity consumption during pressing for high-tech cold press were obtained from an environmental assessment for 3-ply glue (van der Lugt, Vogtlander and Brezet 2012). The electricity consumption for low-tech cold press is assumed to be zero. The electricity consumption for the high-tech hot press step was obtained from an environmental assessment of glue laminated timber products and assumed to be the same for bamboo (Puettmann, Oneil and Johnson 2013). The total electricity consumption for each pressing technique is the sum of the electricity consumed in process steps 1-15 in Table 1.

The carbon footprint is measured as kg of CO_2 equivalent ($kgCO_2e$). Electricity is assumed to be from the local grid (modern coal fired power plant, 0.805 $kgCO_2e/kWh$) to obtain $kgCO_2e/FU$ and then multiplied by the weight of material to obtain $kgCO_2e$. Glue laminated timber boards and laminated veneer lumber (LVL) are also produced by high-tech hot press, so the same electricity consumption of these wood composite products is assumed to be the same as high-tech hot pressed bamboo. However the density of these wood products is different, which factors into the $kgCO_2e$. The cumulative electricity consumption for each pressing method and carbon footprint for bamboo and wood composites is presented in Table 2.

The compressive strength, elastic modulus, and modulus of rupture for bamboo glue pressed composites formed using each class of pressing technique and wood composites were obtained from the literature; details are provided in the Appendix. Figures 39 plots the mechanical properties of bamboo and wood composites with respect to their carbon footprint. Also plotted are the corresponding mechanical properties for a

Guadua density of 400 kg/m^3, which is the average fiber density through the bamboo culm. This corresponds to the mechanical properties of raw bamboo culm, and allows for comparison between processed and unprocessed bamboo for construction.

Table 2: Carbon footprint for manufacture of bamboo or wood composite

Pressing process	Materials	Electricity consumption in manufacture (kWh/FU)	Carbon FP $kgCO_2e$/ FU	Density kg/m^3	Carbon FP $kgCO_2e$
Low-tech cold-press	3-ply bamboo laminate	39.15	31.51	700	0.76
High-tech cold-press	3-ply bamboo laminate	45.17	36.36	700	0.87
High-tech hot-press	3-ply bamboo laminate	52.44	42.21	700	1.01
High-tech hot-press	Glue laminated timber	52.44	42.21	560	1.26
High-tech hot-press	LVL	52.44	42.21	606	1.17

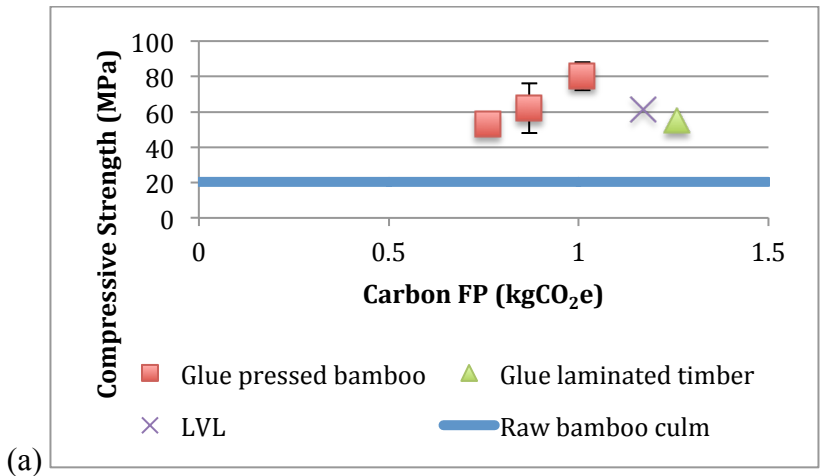

(a)

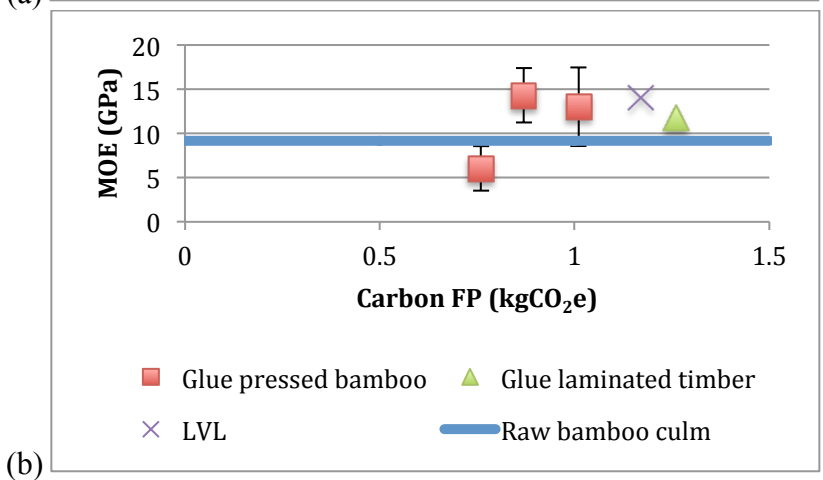

(b)

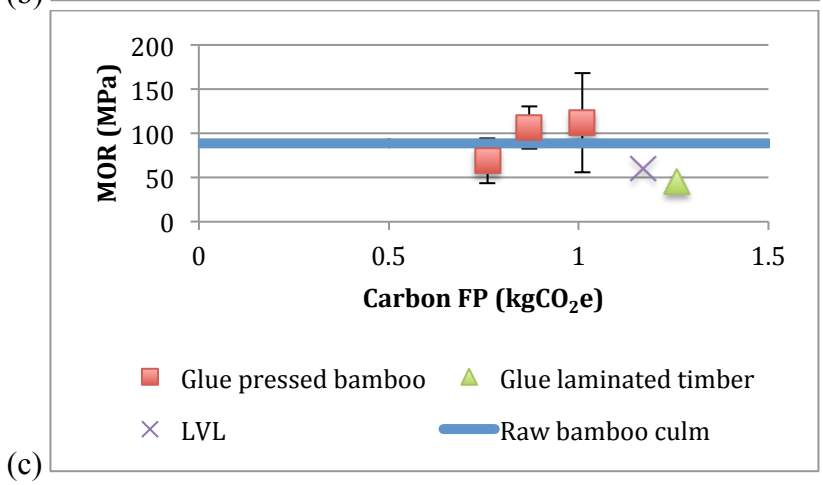

(c)

Figure 39: Compressive strength (a), MOE (b), and MOR (c) of bamboo and wood composites with respect to their carbon footprint from the manufacturing process in comparison to measured mechanical properties for whole Guadua culms

Overall, low-tech cold pressed composites had the poorest mechanical properties, which were often even lower than those of the raw bamboo culm. However, changing the

pressing technique to high-tech cold pressed improved the average compressive strength by 10 MPa, the MOE by a factor of 2, the MOR by nearly 40 MPa. Adding heat to the pressing process improved the average compressive strength by approximately 20 MPa but did not significantly change the MOE or MOR. In comparison to both LVL and glue laminated timber, high tech heat pressed bamboo composites had a lower carbon footprint as a result of electricity consumption in manufacturing, but had significantly higher compressive strength and MOR and comparable MOE. Therefore SBP offer a mechanical advantage in comparison to raw bamboo culms and wood composites and consume less electricity during the manufacturing process. The true impact from the exhaustion of energy also factors in gasoline consumption from transportation, which will depend on whether the bamboo or wood are processed and utilized close to their source.

Conclusion

This study evaluated how mechanical properties of Guaduaa vary with height and radially in the culm. The fiber area fraction was found to correlate directly with the density. Compression tests of small radial sections did not show a strong linear correlation between the MOE and density. In contrast, the compression strength was found to vary linearly with density as would be predicted by the rule of mixtures model. Also in accordance with rule of mixtures, the results from 3-point bending also show a linear correlation between the MOE and MOR with respect to density. Finally nanoindentation experiments were conducted to confirm that the properties of pure bamboo fiber were independent of position.

A study of the environmental feasibility compared the electricity consumption in manufacture of glue pressed bamboo composites to that of wood composites and evaluated if additional energy input correlated to improved mechanical performance of the bamboo composite. The results show that the use of a high-tech cold press technique results in significantly higher MOE, MOR, and compressive strength in comparison to low-tech cold press bamboo composites and even raw bamboo culms. The results also showed that bamboo composites require less electricity input in manufacture than wood composites and that bamboo composites have superior mechanical properties. This study supports the use of SBP for structural applications, although for a full ecological impact the energy input from transportation of materials from cultivation to processing to use also needs to be taken into account.

References

1. Amada, Shigeyasu, Yoshinobu Ichikawa, Tamotsu Munekata, Yukito Nagase, and Hiroyuki Shimizu. "Fiber texture and mechanical graded structure of bamboo." *Composits. Part B, Engineering* 28B (1997): 13-20.

2. Ambrose, J., and D. Vergun. *Design for earthquakes.* New York: John Wiley & Sons, Inc, 1999.

3. ArchDaily. *Passive House / Karawitz Architecture.* 10 28, 2010. http://www.archdaily.com/84165/passive-house-karawitz-architecture/ (accessed 04 17, 2013).

4. Auth, Stefan. *Straw-covered bamboo huts of the Akha Meuo tribe in the traditional mountain village of Ban Chakhampa, Phongsali Province, Laos, Southeast Asia.* 05 13, 2008. http://www.tradebit.com/filedetail.php/4038337v2961523-straw-covered-bamboo-huts-of-the-akha-meuo (accessed 04 17, 2013).

5. Cai, Zhiyoung, and Robet J. Ross. "Mechanical Properties of Wood-Based Composite Materials." In *Wood Handbook, Wood as an Engineering Material*, 12-1-12-12. Forest Products Laboratory, 2010.

6. Correal, Juan F, and Luis F. Lopez. "Mechanical properties of colombian glued laminated bamboo." *Modern Bamboo Structures.* London: Taylor & Francis Group, 2008. 121-127.

7. de Vos, Valentijin. "Bamboo for Exterior Joinery." BSc Thesis, International Timbertrade, Larenstein University, 2010.

8. Garcia, Lina M. *Radial and longitudinal variation of the mechanical properties of bamboo.* BSc Thesis, Cambridge: MIT, 2011.

9. Garcia-Saenz, Martha. "Social and Cultural Aspects of Constructions with Bamboo." *10th Latin American and Caribbean Conference from Engineering and Technology.* Panama City, 2012. 1-7.

10. Gardner, Ana, and Elizabeth Vogel. *Bamboo Biodiversity.* 2006. http://www.eeob.iastate.edu/research/bamboo/maps.html (accessed 04 17, 2013).

11. Gerhardt, Michael R. *Microstructure and mechanical properties of bamboo in compression.* BSc Thesis, Materials Science and Engineering, MIT, Cambridge: MIT, 2012.

12. Gratani, Loretta, Maria Fiore Crescente, Laura Varone, Giuseppe Fabrini, and Digiulio Elepnora. "Growth pattern and photosynthetic activitiy of different bamboo species growing in the Botanical Garden of Rome." *Flora* 203 (2008): 77-84.

13. Kai, Z, and C Xuhe. *Potential of Bamboo-based Panels Serving as Prefabricated Construction Materials.* INBAR, 2009.

14. Khanna, Ajay. *The Temporary Cathedral in structural bamboo, Pereira, Colombia, 1999 by Simon Velez.* 06 29, 2009. http://thesimonvelezfoundation.wordpress.com/about/ (accessed 04 17, 2013).

15. Li, Hongbo, and Shengping Shen. "The mechanical properties of bamboo and vascular bundles." *Journal of Materials Research* 26, no. 21 (10 2011): 2749-2756.

16. Liese, Walter. "Anatomy and Properties of Bamboo." Bamboo Workshop, Hangzhou, 1985.

17. Lugt, van der, Vogtlander, Joost Pablo, and Han Brezet. *Bambo, a Sustainable Solution for Western Europe; Design Cases, LCAs and Land-use.* Technical Report, Delft University of Technology, Delft: International Network of Bamboo and Rattan, 2009.

18. Mahdavi, M, P.L. Clouston, and S.R. Arwade. "A low-technology approach toward fabrication of Laminated Bamboo Lumber." *Construction and Building Materials*, 2012: 257-262.

19. Mahdavi, M, P.L. Clouston, and S.R. Arwade. "Development of Laminated Bamboo Lumber: Review of Processing, Performance, and Economical Considerations." *Journal of Materials in Civil Engineering*, July 2011: 1036-1042.

20. McCormick, T.P. "Chapter 3: Shear Walls." In *Seismic Training for Building Contractors and Inspectors Participant Handbook*, by Janney, Elstner, and Associates, California Wiss, California Office of Emergency Services, United States Building Industry Association and Federal Emergency Management Agency, 17-48. Governor's Office of Emergency Services, 1995.

21. Nguyen, T.H., and T. Shehab. "Use of bamboo composites as structural members in building construction." In *Challenges, Opportunities and Solutions in Structural Engineering*, by Nader Ghafoori, 605-608. Lonfon: Taylor & Francis Group, 2010.

22. Nogata, Fumio, and Hideaki Takahashi. "Intelligent Functionally Graded Material: Bamboo." *Composites Engineering* 5, no. 7 (1995): 743-751.

23. Nugroho, Naresworo, and Naoto Ando. "Development of structural composite products made from bamboo II: fundamental properties of laminated bamboo lumber." *Journal of Wood Science* 47 (2001): 237-242.

24. PATH. *Prescriptive Method for Structural Insulated Panels (SIPs) Used in Wall Systems in Residential Construction.* Washington, DC: U.S. Department of Housing and Urban Development, 2006.

25. Popular Science. *GluBam Construction | PopSci.* 12 05, 2008. http://www.popsci.com/bown/2008/product/glubam-construction (accessed 04 25, 2013).

26. Puettmann, Maureen, Elaine Oneil, and Leonard Johnson. "Cradle to Gate Life Cycle Assessment of Glue-Laminated Timbers Production from the Southeast." 2013, 1-24.

27. Sulastiningsih, I.M., and Nurwati. "Physical and Mechanical Properties of Laminated Bamboo Board." *Journal of Tropical Forest Science* 21, no. 3 (2009): 246-251.

28. Sweitzer, Jim. *Scanning Electron Microscope.* http://www.purdue.edu/rem/rs/sem.htm (accessed 04 17, 2013).

29. Trujillo, E, L, Van Vuure, AW Osorio, J Ivens, and I Verpoest. "Bamboo (Guadua angustfolia) fibres for strong light composite materials." *IXth World Bamboo Congress.* Antwerp, 2012. 329-338.

30. U.S. Department of Energy. *DOE Solar Decathlon: 2009.* 03 23, 2010. http://www.solardecathlon.gov/past/2009/team_illinois.html (accessed 04 26, 2013).

31. USC Viterbi School of Engineering News. *A full-sized California-style home made of bamboo.* 04 08, 2009. http://viterbi.usc.edu/news/news/2009/bamboo-housing-takes.htm (accessed 04 17, 2013).

32. van der Lugt, P., J.G. Vogtlander, and J.C. Brezet. "Life Cycle Assessment and Carbon Sequestration; the Environmental Impact of Industrial Bamboo Products." *12th World Bamboo Congress.* Antwerp, 2012. 73-85.

33. Verma, C.S., and V.M. Chariar. "Development of layered and laminate bamboo composite and their mechanical properties." *Composites: Part B*, 2011: 1-7.

34. Verma, C.S., and V.M. Chariar. "Stiffness and strength analysis of four layered laminate bamboo composite at macroscopic scale." *Composites: Part B*, 2012: 1-8.

35. Wan, YQ, and FK Ko. "Hierarchial Structure and Mechanical Properties of Bamboo Fiber." Report, Advanced Materials and Process Engineering Laboratory, University of British Columbia, Vancouver, 2011.

36. Wang, Zheng, and Wenjing Guo. *Laminated Panel Manufacture of Two Kinds of Bamboo for Architecture Material and Property Comparison.* Working Paper, Research Institute of Wood Industry, Chinese Academy of Forestry Research, Beijing: INBAR, 2003.

37. Yeh, Min-Chyuan, Wei-Chen Hong, and Yu-Li Lin. "Flexural Properties of Structural Laminated Bamboo/Solid Wood Composite Box Hollow Beams." *Taiwan J For Sci* 24, no. 1 (2009): 41-50.

38. Yu, Yan, et al. "Cell-wall mechanical properties of bamboo investigated by in-situ imaging nanindentation." *Wood and Fiber Science*, 2006: 527-535.

Appendix

Compression testing

Table A1: Average dimensions for compression samples

Sample	Average Length (mm)	Average Width (mm)	Average Thickness (mm)
2E1	17.86	18.66	10.03
2E2	17.47	18.16	8.79
2F1	17.04	18.41	9.29
2F2	17.38	18.16	10.21
2G1	17.57	18.87	8.87
2G2	17.58	18.78	9.97
4D1	17.07	16.44	8.76
4D2	16.84	16.17	8.97
4E1	15.75	18.65	9.59
4E2	16.75	17.84	8.48
4F1	16.38	18.13	8.84
4F2	16.30	17.40	9.15
6I1	14.96	15.17	8.09
6I2	15.31	15.15	8.41
6J1	15.59	16.99	8.55
6J2	15.25	17.12	8.40
20D1	11.18	12.42	6.24
20D2	11.29	12.68	6.41
20E1	11.50	13.08	6.23
20E2	11.36	12.85	6.74
20F1	11.57	12.64	5.93
20F2	11.69	12.65	6.48
20.5D2	12.04	14.82	6.34
20.5E1	11.68	11.50	5.61
20.5F1	10.46	11.51	4.91
20.5F2	10.46	11.56	6.74
22D1	9.30	9.87	5.54
22D2	9.40	10.00	4.85
22E2	9.41	9.76	5.33
22F1	10.39	11.92	5.18
22F2	10.30	11.69	5.50
24D2	9.71	9.93	5.26

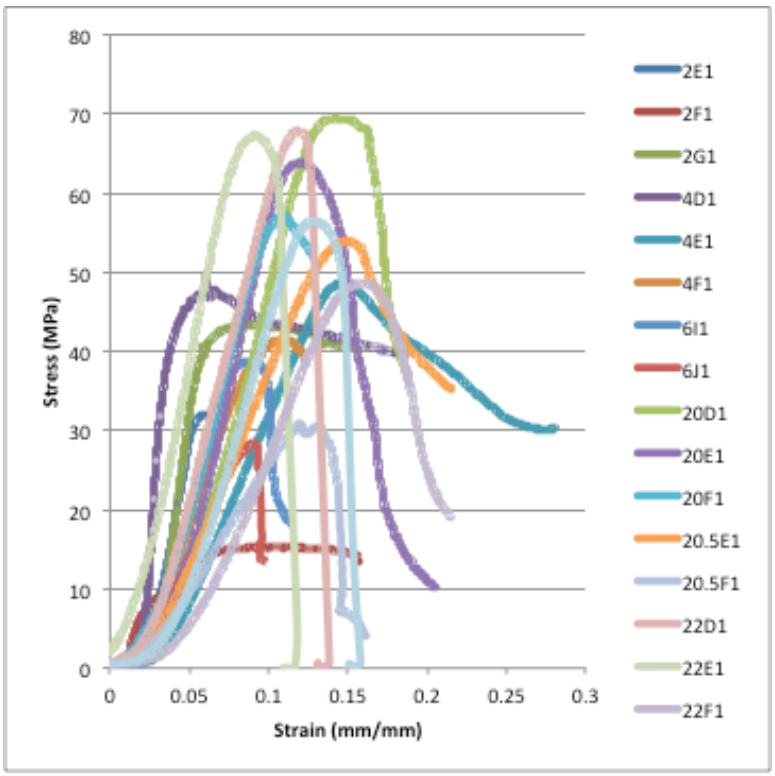

Figure A1: Plot of stress versus strain from compression test of outer radial sections for six internode heights

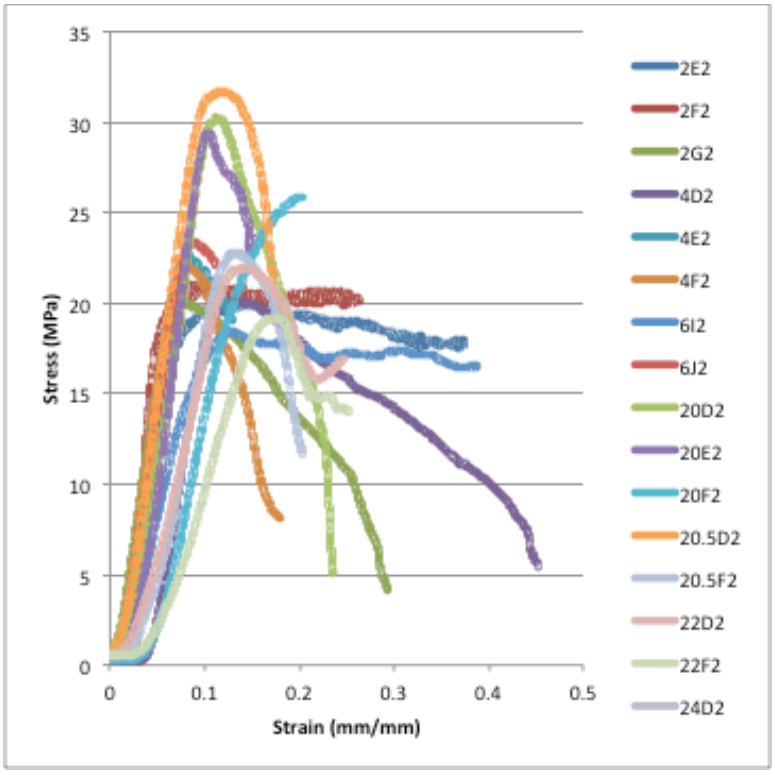

Figure A2: Plot of stress versus strain from compression test of inner radial sections for seven internode heights

Tensile Testing

Table A2: Average dimensions of tensile specimens

	Gauge width (mm)	Gauge thickness (mm)	Length (mm)
6F1	3.73	3.65	101.42
6F3	3.49	2.61	101.42
6F4	3.54	2.88	101.42

Table A3: Value of MOE as measured from plot of stress versus strain from tensile testing

	MOE (GPa)
6F1	4.82
6F3	0.13
6F4	2.75

Bending

Table A4: Average dimensions of bending specimens

	Beam width (mm)	Beam height (mm)
2A1	3.54	4
2A2	3.5	4.69
2A3	3.29	4.4
2A4	3.54	3.6
2B1	3.74	3.58
2B2	3.74	4.64
2B3	3.18	3.25
2B4	3.49	3.58
2C1	3.4	4.05
2C2	3.48	4.91
2C3	3.48	3.58
2C4	3.48	3.58
4A2	3.63	4.79
4A3	2.91	3.18
4A4	3.76	5.12
4B2	3.55	4.3
4B3	3.12	4.22
4B4	3.12	4.22
6D1	3.81	2.4
6D2	3.72	2.71
6D3	4.02	3.71
6G1	3.67	3.48
6G2	3.5	3.08
6G3	3.3	3.69
6G4	3.47	3.87
6H1	3.34	3.12
6H2	3.78	3.99
6H4	3.47	3.86

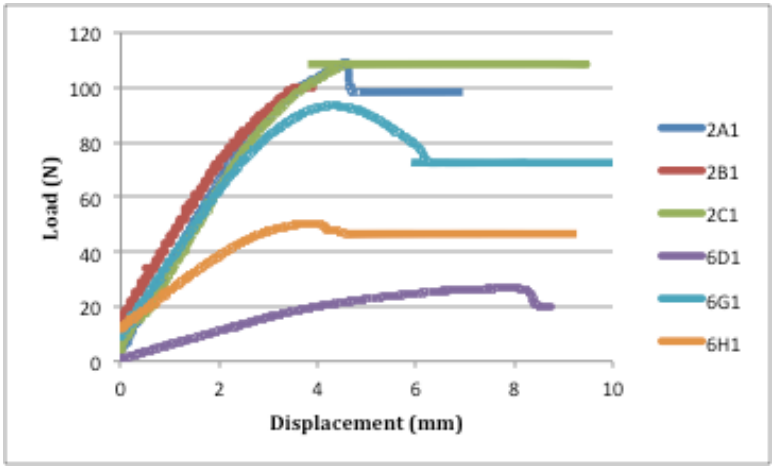

Figure A3: Plot of load versus displacement from 3-point bending test for radial section 1

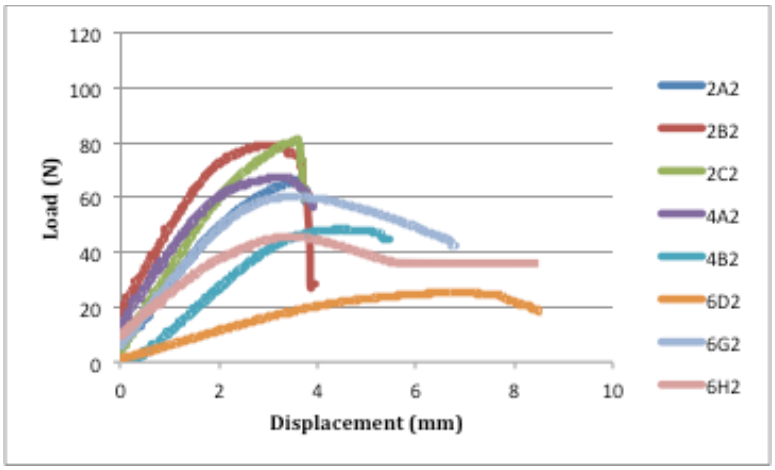

Figure A4: Plot of load versus displacement from 3-point bending test for radial section 2

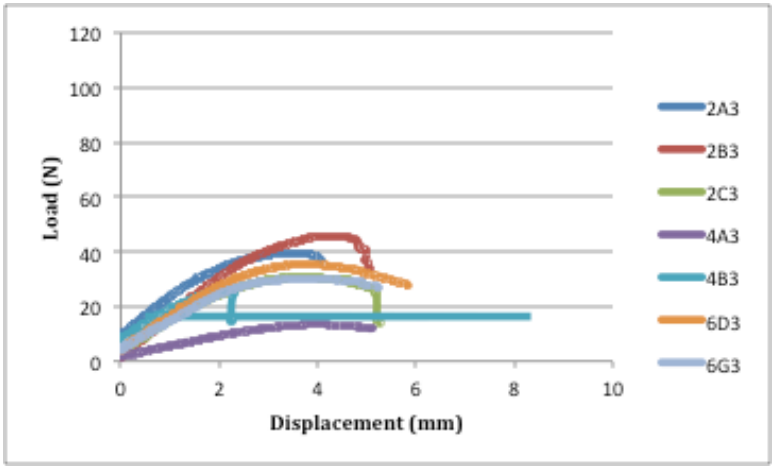

Figure A5: Plot of load versus displacement from 3-point bending test of radial section 3

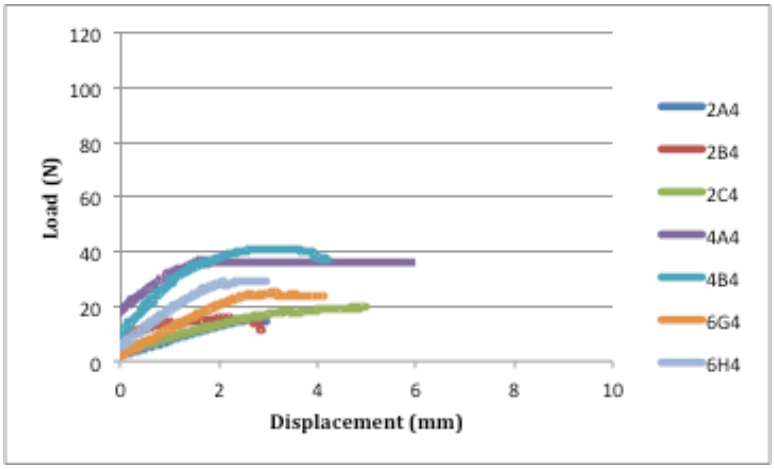

Figure A6: Plot of load versus displacement from 3-point bending test of radial section 4

Environmental Feasibility

Table A5: Mechanical properties for low-tech cold pressed bamboo composite

Compressive Strength (MPa)	MOE (GPa)	MOR (MPa)	Source
-	5.02	-	(Verma and Chariar, Stiffness and strength analysis of four layered laminate bamboo composite at macroscopic scale 2012)
-	4.04	-	(Verma and Chariar, Stiffness and strength analysis of four layered laminate bamboo composite at macroscopic scale 2012)
-	4.6	-	(Verma and Chariar, Stiffness and strength analysis of four layered laminate bamboo composite at macroscopic scale 2012)
-	5.23	-	(Verma and Chariar, Stiffness and strength analysis of four layered laminate bamboo composite at macroscopic scale 2012)
-	3.03	-	(Verma and Chariar, Stiffness and strength analysis of four layered laminate bamboo composite at macroscopic scale 2012)
-	2.21	-	(Verma and Chariar, Stiffness and strength analysis of four layered laminate bamboo composite at macroscopic scale 2012)
-	4.36	-	(Verma and Chariar, Stiffness and strength analysis of four layered laminate bamboo composite at macroscopic scale 2012)
-	5.14	-	(Verma and Chariar, Stiffness and strength analysis of four layered laminate bamboo composite at macroscopic scale 2012)
-	5.46	-	(Verma and Chariar, Stiffness and strength analysis of four layered laminate bamboo composite at macroscopic scale 2012)
-	5.94	-	(Verma and Chariar, Stiffness and strength analysis of four layered laminate bamboo composite at macroscopic scale 2012)
-	9.3	76.5	(Mahdavi, Clouston and Arwade, A low-technology approach toward fabrication of Laminated Bamboo Lumber 2012)
55.39	10.03	95.06	(Sulastiningsih and Nurwati 2009)
50.87	9.48	45.35	(Sulastiningsih and Nurwati 2009)
56.09	9.81	87.8	(Sulastiningsih and Nurwati 2009)
49.34	7.26	38.61	(Sulastiningsih and Nurwati 2009)

Table A6: Mechanical properties for high-tech cold pressed bamboo composite

Compressive Strength (MPa)	MOE (GPa)	MOR (MPa)	Source
47.6	19.14	-	(Correal and Lopez 2008)
-	10.74	104.9	(Yeh, Hong and Lin 2009)
-	11.25	124.9	(Yeh, Hong and Lin 2009)
80	16	128.8	(Verma and Chariar, Development of layered and laminate bamboo composite and their mechanical properties 2011)
55	14.5	68.28	(Verma and Chariar, Development of layered and laminate bamboo composite and their mechanical properties 2011)
66	14.3	105.74	(Verma and Chariar, Development of layered and laminate bamboo composite and their mechanical properties 2011)

Table A7: Mechanical Properties of high-tech hot pressed bamboo composite

Compressive Strength (MPa)	MOE (GPa)	MOR (MPa)	Source
85.47	13.68	174.70	(Wang and Guo 2003)
71.99	10.5	135.78	(Wang and Guo 2003)
89.42	23.48	210.23	(Wang and Guo 2003)
82.42	19.72	194.96	(Wang and Guo 2003)
72	10.97	75	(Nguyen and Shehab 2010)
-	9.43	62.66	(Nugroho and Ando 2001)
-	10.30	69.33	(Nugroho and Ando 2001)
-	10.50	67.57	(Nugroho and Ando 2001)
-	11.87	83.45	(Nugroho and Ando 2001)
-	12.06	86.00	(Nugroho and Ando 2001)
-	10.89	74.04	(Nugroho and Ando 2001)